Cholesteric Liquid Crystal Systems

Shining Light on Helix Deformation
Reflecting on Photonic Band Gaps

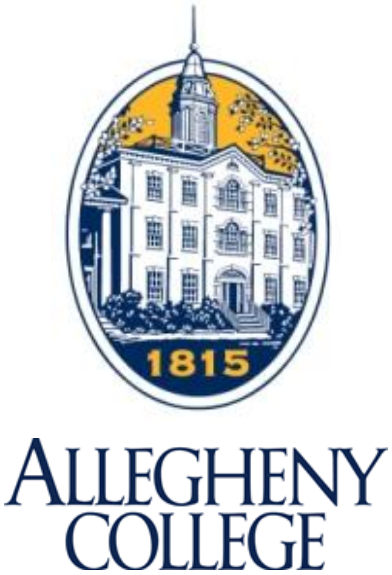

Daniel R Brennan

Department of Physics

Senior Comprehensive Project

Advisor: Dr. David Statman

2nd Reader: Dr. Jamie Lombardi

April 22, 2011

Cholesteric Liquid Crystal Systems

Shining Light on Helix Deformation
Reflecting on Photonic Band Gaps

Allegheny College

Department of Physics

Senior Comprehensive Project

Advisor: Dr. David Statman

2nd Reader: Dr. Jamie Lombardi

April 22, 2011

Submitted to the Allegheny College Department of Physics

to partially fulfill the requirements for the degree of

Bachelor of Science

I hereby recognize and pledge to fulfill my responsibilities, as defined by the Honor Code, and to maintain the integrity of both myself and the College community as a whole.

Pledge: _____

Daniel Ryan Brennan

Acknowledgements

Dr. David Statman: Thanks for all the help and guidance throughout my time at Allegheny College, with class work, comp work, grad school, developing good taste in beer and Hungarian food, and everything else! I have certainly learned a lot of awesome things from you. Oh, and thanks for making us have fun in lab, we all had a great time.

Dr. Jamie Lombardi: Haha, I still remember my first encounter with the alligator on a spring and a bunch of other great things from your classes, that's how you know you're a great teacher. To the best second reader and one of the best teachers I have ever had, thank you!

My Family: You crazy hooligans make me look sane, but I love you all. I know you guys may not understand some of the next 60 pages, but you'll read it anyways and be happy for me and proud of me, which is the most wonderful thing ever. Thank you!

Physics Family: Thanks for all the facebook hacking, the practical jokes, the physics parties, the jig saw puzzle showdowns, baby monkey riding on a honey badger, and the general craziness/absurdity that went on in lab, it made for a grand year and lots of good times.

Shivani: Consider yourself acknowledged… for being the best person in the world for putting up with me. Thanks for being understanding, helpful, and fun when I needed it most and thanks for reminding me that I should probably sleep now and then. Apple business approves. Allegheny wouldn't be the same without you. :D

Table of Contents

Abstract……01

Introduction……02

Background Theory……03

Experimental Method……20

Experimental Results and Analysis……25

Discussion and Conclusions……50

Future Work……52

References……53

Appendix A - Sample Preparation……54

Abstract

The characteristic photonic band gap exhibited by cholesteric liquid crystal systems has been shown to be quite dynamic in nature. As a result of this, it is possible to employ various physical stimuli to broaden and/or shift the spectrum of wavelengths of light reflected by the sample. This research is an investigation into the process through which polarized laser light and/or temperature effects change in the helix (and therefore the photonic band gap) of dye doped cholesteric liquid crystal systems. Phenomena such as helix flattening, surface gliding, temperature induced pitch changes, and the effects of trans-cis methyl red dye isomerization have been theoretically modeled and evaluated with Stokes Polarimetry and UV-Vis spectroscopy. Results show that helical flattening due to the pump beam's electric field is inconsequential, yet changes in samples' structures brought about by temperature, surface director rotation, and what may be the cis isomer of methyl red dye acting as a chiral doping agent, show up as significant factors in determining the photonic band gap and structure of a cholesteric liquid crystal system.

Introduction

Liquid crystalline materials are an interesting field of study with broad implications in the creation and development of technologies like temperature sensors, photonic crystals, liquid crystal displays, optical switches, 3D displays, and even artificial muscles, to name a few. This diverse array of technological applicability arises from the unique characteristics inherent in liquid crystal (LC) systems. The properties of LCs arise, at least in part, from the fact that they behave like both a liquid and a crystal, because the molecules that compose this kind of material are free to move past one another, yet also have long range orientational and sometimes positional order. Because of this broad definition though, there are many substances that can be classified as a LC, and they can come in many different shapes, structures, and states. Furthermore, each of these LC subcategories can have its own distinct set of properties. This research, however, will study only one specific branch of the liquid crystal family.

Research will be focused on calamitic, or rod shaped, LCs that are thermotropic in nature, meaning that they undergo temperature dependent phase changes. Thermotropic LCs are organically base molecules that can occupy different phases, anywhere from isotropic liquids (at higher temperatures), to entirely crystalline solids (at lower temperatures). However it is only the intermediate states, called mesophases, which exhibit liquid crystalline properties. Thermotropic LCs have three main mesophases: nematic, smectic, and cholesteric (or chiral nematic). [1] LCs in the nematic state lack positional order, but have orientational order, like toothpicks in a long box. The smectic phase has directional and 1D positional (layered) ordering. Finally, the cholesteric phase has an average orientational order that rotates slightly through successive layers of the sample, although each layer still has a nematic ordering. This characteristic makes the LC molecules sweep out a helix as you go through the sample. A depiction of the cholesteric liquid crystal (CLC) structure is shown in *Figure 1* on the following page. The focus of this research will deal solely with calamitic thermotropic LCs in the cholesteric phase.

CLCs interact in an especially interesting way with light. For reasons that will be explored in depth later on, this kind of LC system selectively reflects circularly polarized light of the same handedness and wavelength as that of the sample's helix and pitch, respectively. (The pitch is the length along the helix it takes for the LCs to sweep out a full 360 degree revolution.) The result is a photonic band gap, where light of a specific handedness and range of wavelengths is selectively reflected. Since the pitch of a CLC's helix affects this range of wavelengths, learning the mechanisms through which the pitch of the sample change should allow us to better devise methods to tune the photonic band gap. This topic is the focus of my research, and it has implications for the creation of such technologies as tunable mirrorless lasers, photonic crystals, and 3D CLC displays.

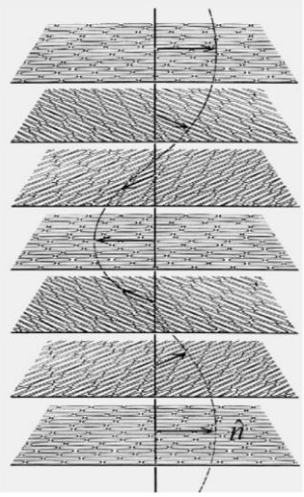

Figure 1: Chiral nematic liquid crystal structure through successive layers.

Background Theory

The behavior of the CLC sample, and consequently the light that travels through it, is affected by many factors, but one of the most important of these stems from the anisotropy of the CLC sample. Calamitic LCs in the nematic state are anisotropic because they have a long axis and an average orientation, called the director, $\hat{n}$, along which the molecules generally point. This is important because it will be easier for charge to rearrange itself to opposite ends of the long axis of the LC molecule than it will for the short axes. This difference in polarizability gives the LC molecules different dielectric constants and refractive indices in different directions. Since all the LC molecules in the nematic state align in the general direction of the director, the entire bulk of the sample will exhibit the anisotropic properties of its constituent molecules.

The net polarization of a LC sample can vary because of the interaction and/or presence of permanent and induced dipoles. The strength of the permanent dipole of a LC depends on the

functional groups attached to the LC mesogen (the main body component of a LC that induces order). Furthermore, this dipole can be enhanced or diminished by the presence of an electric field aligned parallel or antiparallel to the director, respectively. The net polarization, $\vec{P}$, of the LC sample, induced by an electric field, can be calculated from knowledge about the LC's properties

$$\vec{P} = \varepsilon_0 \vec{\vec{\chi}} \vec{E} \qquad \text{or} \qquad \begin{pmatrix} P_x \\ P_y \\ P_z \end{pmatrix} = \varepsilon_0 \begin{pmatrix} \chi_\perp & 0 & 0 \\ 0 & \chi_\perp & 0 \\ 0 & 0 & \chi_\parallel \end{pmatrix} \begin{pmatrix} E_x \\ E_y \\ E_z \end{pmatrix}, \tag{1}$$

where ε_0 is the permittivity of free space, $\vec{E}$ is the applied electric field, and $\vec{\vec{\chi}}$ is the electric susceptibility tensor (a measure of how easily a material can be polarized). The electric displacement of the material is determined by its polarization and the applied electric field

$$\vec{D} = \varepsilon_0 \vec{E} + \vec{P}. \tag{2}$$

Combining and simplifying *Equations 1* and *2*, we obtain

$$\vec{D} = \vec{\vec{\varepsilon}} \vec{E}, \tag{3}$$

where $\vec{\vec{\varepsilon}} = \varepsilon_0 \varepsilon_r$ is the permittivity tensor of the material, and $\varepsilon_r = 1 + \vec{\vec{\chi}}$. Since the dielectric constant of nematic LCs is different along the directions parallel and perpendicular to the director, we can write

$$\Delta\varepsilon_r = \varepsilon_{r\parallel} - \varepsilon_{r\perp}, \tag{4}$$

where $\Delta\varepsilon_r$ is the difference between the dielectric constants parallel and perpendicular to the long axis of the LC molecule.

The effects of an electric field go beyond merely enhancing or diminishing the dipoles in LC molecules. The electric field also exerts a torque, $\vec{N}$, on the dipoles in the LC molecules of the sample

$$\vec{N} = \vec{p} \times \vec{E}, \tag{5}$$

where $\vec{p}$ is the dipole in the liquid crystal molecule. In such an electric field, the liquid crystal molecules align themselves as much as possible in a direction parallel to the field to reduce the energy of the

system. The presence of an electric field can actually serve to reorient the bulk of the liquid crystal sample. This torque exemplifies a mechanism through which we can effect change in the helix of a CLC sample. There are, however, other factors that determine how liquid crystals behave both in the absence and under the influence of an electric field, but in all cases, the LC molecules tend towards minimum system energy.

A powerful tool for evaluating the behavior of a LC sample lies in free energy minimization, but determining the free energy of a CLC system can be tricky because it is affected by many factors. One contribution to the free energy of a sample comes from the interactions of azo-dyes with LC molecules. Azo-dyes are frequently added to LC samples because of the dramatic enhancement effect they have in reorienting the director of LC molecules when exposed to laser light. [2] These dyes have a similar structure to LCs, yet when excited they can undergo trans-cis or cis-trans isomerization. This is significant because dye molecules in the trans conformation have a linear shape, where those in the cis conformation are more curled up, almost in the shape of a V, as is shown in *Figure 2*:

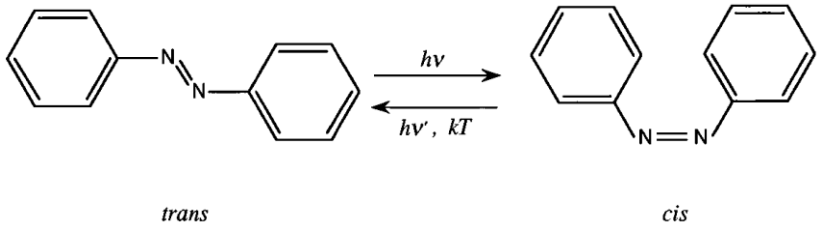

Figure 2: Trans and cis conformations of an azo-dye backbone.

The probability of trans-cis isomerization for azo-dyes exposed to polarized laser radiation around 440 nm increases when the orientation of the N=N bond lies closer to the orientation of the optical field. [3] [4] Since the cis state is only meta-stable, the dye molecules eventually relax back to their trans state, facilitated through ambient thermal energy or photoexcitation. When the azo-dye comes back to the trans state, it will have a more or less randomized orientation, yet molecules oriented close to or along the direction of the laser's polarization will be excited once again, while those oriented perpendicular to

it will no longer become photoexcited. This mechanism drives the net reorientation of trans dye molecules so that they are orthogonal to the optical field, which in turn reorients the LC molecules (since they are both rod shaped and can possess dipoles). This reorientation only happens near the irradiated surface though, because the laser emission is absorbed by the dye before it can transmit through the entire thickness of the sample. Through this dynamic, then, the system tends to minimize energy through director reorientation at the irradiated surface, which in turn induces a twist in the director throughout the thickness of the sample. This phenomenon is characteristic of standard nematic LC systems, but the process is very similar to what happens in CLC systems.

The reason that one side of the LC sample can reorient, due to the effects of an optical field, while the other remains immobile, lies in the phenomena of surface anchoring. This is the process whereby LC molecules become bonded or otherwise held in a particular direction relative to the surface of the glass cell that contains the LC sample. Prior to filling a sample with LC, the surfaces of these glass slides are usually etched to produce fine grooves, or coated with some type of polymer that can be oriented through a mechanical process like rubbing or photopolymerization. When such mechanisms are in place and the sample is filled, the LC molecules will usually align themselves with the direction of the grooves or polymer because of interactions of the LCs with the topology of the surface, or intermolecular interactions arising from sterics, polarity, or Van der Waals bonding. [5] This serves to set the director orientation for the LC sample, and anchor it there. It also sets the direction that the LCs will prefer to come back to after a deformation is introduced; this is called the easy axis of the sample. This is different from the director of the sample, which can be thought of as the general direction the LCs are oriented in at a particular time, and not necessarily their preferred direction. However, both the director and the easy axis of a sample can be reoriented due to effects from the optical field of light. Overall, this phenomenon is important because it contributes to the free energy at the surfaces of the sample, but it is of particular importance to CLC samples because, in general, the director will sweep out a continuous

helix whose ends line up with the surface anchoring at the edges of the sample. This ultimately has an impact on how many pitch lengths will fit inside a CLC sample. There are other factors that help determine the chirality of the CLC sample as well, one of which is the presence of chiral doping agents.

Chiral doping agents are merely chiral additives that are homogeneously mixed in with an untwisted nematic LC to make it into a CLC. These additives only serve to induce the cholesteric structure. The higher the concentration of these chiral agents, the shorter the pitch of the sample will be (and vice versa). This means that we also have to consider the interactions of these chiral agents with the bulk of the LCs when trying to determine the free energy of the sample.

Given these contributions to the free energy from azo-dyes, bulk distortions, reorientations, surface anchoring, and the chiral doping agent, we can now determine a free energy function that will accurately model a CLC sample and its interactions with optical fields. Furthermore, the minimization of this function will tell us how the sample behaves, because all of these dynamics will tend towards minimum energy. The free energy per unit volume of a nematic LC can be modeled like a spring with three terms for specific distortions or reorientations called bends, twists, and splays [6]

$$F_V = \frac{1}{2}K_1\left[\nabla\cdot\hat{n}\right]^2 + \frac{1}{2}K_2\left[\hat{n}\cdot\left(\nabla\times\hat{n}\right)\right]^2 + \frac{1}{2}K_3\left[\hat{n}\times\left(\nabla\times\hat{n}\right)\right]^2, \tag{6}$$

where $\hat{n}$ is the director, K_1, K_2, and K_3 have units of Newtons, and are analogous to spring constants for bend, twist, and splay distortions (respectively).

This situation changes with CLC samples because it is necessary to include an extra term to account for the presence of intermolecular chiral interactions

$$F_V = k_2\left[\hat{n}\cdot\left(\nabla\times\hat{n}\right)\right] + \frac{1}{2}K_1\left[\nabla\cdot\hat{n}\right]^2 + \frac{1}{2}K_2\left[\hat{n}\cdot\left(\nabla\times\hat{n}\right)\right]^2 + \frac{1}{2}K_3\left[\hat{n}\times\left(\nabla\times\hat{n}\right)\right]^2, \tag{7}$$

where k_2 is another elastic constant, but with units of Newtons/meter. Assuming a right handed helix with its axis pointing along the *z* direction, the *x* and *y* directions in the plane of the sample, and surface anchoring along the *x* direction, the director can be expressed as

$$\hat{n} = \begin{pmatrix} \cos(\varphi) \\ \sin(\varphi) \\ 0 \end{pmatrix} \quad \text{where} \quad \varphi = 2\pi \frac{z}{P_0}, \tag{8}$$

where φ is the angle the director makes with respect to the x axis, and P_0 is the pitch at equilibrium. Evaluating the divergence and curl of $\hat{n}$ through a full pitch length, and plugging these values into *Equation 7* yields

$$F_V = -k_2 q_0 + \frac{1}{2} K_2 {q_0}^2, \tag{9}$$

where $q_0 = \frac{2\pi}{P_0}$ is the wavevector of the CLC helix (alternatively, it can be thought of as the chirality of the helix). The only terms left describe the twist distortion and chirality free energy terms. This is the case for all CLC systems that we will be working with, because splay and twist distortions are not naturally present in CLC samples, and the optical field we will be using does not induce these deformations. [6] The minimum F_V can be determined by taking the derivative of this function with respect to q_0 and setting it equal to zero

$$\frac{dF_V}{dq_0} = -k_2 + K_2 q_0 = 0. \tag{10}$$

From this result it is apparent that $q_0 = k_2 / K_2$, so we can make the following conclusions:

$$P_0 = \frac{2\pi K_2}{k_2}, \tag{11}$$

$$F_V = -\frac{1}{2} \frac{{k_2}^2}{K_2}. \tag{12}$$

We can tell from *Equations 11* and *12* that the minimum free energy (MFE) of the CLC system is lower than that of a standard nematic LC, which would normally be equal to zero (because the chiral elastic constant, k_2, would be zero). From this we can conclude that the CLC system is at MFE when there is a

certain degree of chirality present. Such a state would raise the energy of a normal nematic LC structure, but the presence of chiral doping agents in CLCs shifts the equilibrium towards a twisted state. Furthermore, we can say that the equilibrium pitch at MFE is determined by the ratio between the twist and chirality elastic constants, and that any distortions in the helix would necessarily change the chirality and twist components of the free energy function, thereby raising the energy of the system.

This free energy per unit volume model can be expanded to include the interactions of an optical field with LC molecules [6], azo-dyes [6], and surface anchoring [7] by adding extra terms to *Equation 9* that account for the energies of these interactions. (In this case though, we will use a generic $d\varphi/dz$, or equivalently φ', instead of q_0.) This new function can be expressed for a sample of thickness L as

$$F_V = -k_2(\varphi') + \frac{1}{2}K_2(\varphi')^2 + \frac{1}{2}I\eta\sin^2(\delta\varphi_p) + \frac{1}{2}W_0\cos^2(\delta\varphi_0) + \frac{1}{2}W_L\cos^2(\delta\varphi_L), \qquad (13)$$

where I is the intensity of the incident radiation, η is a constant with units of seconds(meters) that relates the intensity of the incident radiation to the reorientations that the radiation causes in the dye, $\delta\varphi_p \equiv \varphi - \varphi_p$ is the difference in angle between the director and the polarization of the optical field, W_0 and W_L are surface anchoring energy constants at surfaces 0 and L (respectively) with units of Newtons, and $\delta\varphi_0 \equiv \varphi - \varphi_0$ and $\delta\varphi_L \equiv \varphi - \varphi_L$ are the difference in angle between the director and the easy axis at surfaces 0 and L (respectively). To get the total MFE of the system, it is necessary to integrate the chiral, twist deformation, and director-dye-optical field interactions throughout the length of the sample to account for the energy of the entire sample. It is not necessary to do this integration over the surface anchoring terms because they aren't present in the bulk of the sample, these terms just have to be added outside of the integral. *Equation 13* can then be used to determine how the system will tend towards, and behave at, the system's MFE.

The Euler-Lagrange method for the minimization of a function can be employed to determine

the MFE of the system. After the derivative of the total free energy is taken with respect to an arbitrary variable, α, we obtain (*Equation 14*)

$$\frac{dF_V}{d\alpha} = \int_0^L \left[I\eta \sin\left(\delta\varphi_p\right)\cos\left(\delta\varphi_p\right) - K_2\left(\varphi''\right)\right]\frac{d\varphi}{d\alpha}dz + \left(K_2\varphi' - k_2\right)\frac{d\varphi}{d\alpha}\bigg|_0^L + \frac{d}{d\alpha}\left(\frac{1}{2}W_0\cos^2\left(\delta\varphi_0\right) + \frac{1}{2}W_L\cos^2\left(\delta\varphi_L\right)\right) = 0.$$

Since this entire function must reduce to zero, we can set related terms equal to zero. The resulting functions can be simplified further by noting that the difference in angle between the easy axis and director at either surface ($\delta\varphi_0$ and $\delta\varphi_L$) will be small, because the easy axis glides with the director. This process yields the following relations

$$K_2\varphi'' = \frac{1}{2}I\eta\sin\left(2\delta\varphi_p\right), \tag{15}$$

throughout the bulk, and

$$\frac{K_2}{W_0}\varphi_0' = \varphi - \varphi_0, \tag{16}$$

$$\frac{K_2}{W_L}\varphi_L' = \varphi - \varphi_L, \tag{17}$$

at the surface. These equations can be utilized, in conjunction with experiments that measure director reorientations in a CLC sample exposed to varied intensities of polarized laser emission, to determine properties of CLC systems. Appropriate procedures and analysis can yield values for the anchoring energy coefficients, W_0 and W_L, at each surface, or the constant η. This information is helpful in determining the time evolution of LC structures exposed to laser emission, because it further refines our MFE model. Now that the MFE model of a CLC system is sufficiently sophisticated, we can use it to model the behavior of a CLC sample under exposure to laser emission.

When a CLC sample is exposed to an optical field, the helix should flatten because of the reorientation effects discussed earlier. [6] This happens because the director sweeps out a circle throughout the bulk, making all angles with the optical field. Those angles more closely aligned to the optical field will experience reorientations because of trans-cis isomerization, and those less aligned will

not experience as much reorientation. This process lengthens the part of the helix perpendicular to the field and shortens segments of the helix parallel to the field, which in turn lengthens the pitch of the helix. This behavior continues as the strength of the optical field is increased, creating a nearly nematic LC structure with short 'walls' where the director flips 180 degrees. As the strength of the field increases further, these walls become further and further apart, eventually leading to a complete unwinding of the CLC helix.

To evaluate this behavior, we will need to assume a fairly uniform electric field throughout the thickness of the sample. This is a decent approximation because the samples are approximately 1.5 μm thick. Given a helix with its axis along the *z* direction, a director in the *x-y* plane, and an electric field along the *y* axis, we can say that the energy per unit volume is [6]

$$U = -k_2(\varphi') + \frac{1}{2}K_2(\varphi')^2 - \frac{1}{2}\varepsilon_0\Delta\chi_e E^2\sin^2(\varphi) + \frac{1}{2}W_0\cos^2(\delta\varphi_0) + \frac{1}{2}W_L\cos^2(\delta\varphi_L), \qquad (18)$$

where the third term describes the LC-field interaction. In *Equation 18*, ε_0 is the permittivity of free space, $\Delta\chi_e$ is the difference in electric permittivity between the long and short axes of the LC molecule, and E is the applied electric field. *Equation 18* can be simplified to

$$U_1 = \frac{1}{2}K_2(\varphi' - q_0)^2 - \frac{1}{2}\varepsilon_0\Delta\chi_e E^2\sin^2(\varphi) + \frac{1}{2}W_0\cos^2(\delta\varphi_0) + \frac{1}{2}W_L\cos^2(\delta\varphi_L), \qquad (19)$$

where U_1 differs from U by a constant equal to $\frac{1}{2}K_2{q_0}^2$, and the equilibrium chirality, chirality q_0, is equal to $\mathrm{q}_0 = k_2/K_2$ (as was found from *Equation 11*). The free energy per unit volume for a cross section of sample orthogonal to the helix is equivalent to the integral of U_1 along the length of the *z* axis occupied by that cross section. The minimization of this free energy function follows the same procedure as the minimization of *Equation 13*; the result of which is

$$\xi^2\varphi'' + \sin(\varphi)\cos(\varphi) = 0, \qquad (20)$$

where

$$\xi^2 = \frac{K_2}{\varepsilon_0 \Delta\chi_e E^2}\,. \tag{21}$$

If *Equation 20* is multiplied by φ' and integrated, we obtain

$$\frac{1}{2}\xi^2(\varphi')^2 + \frac{1}{2}\sin^2(\varphi) = \frac{1}{2\kappa^2}\,, \tag{22}$$

where $\frac{1}{2\kappa^2}$ is an integration constant. If this then is solved for φ', we see that

$$\varphi' = \frac{1}{\xi\kappa}\sqrt{1-\kappa^2\sin^2(\varphi)}\,. \tag{23}$$

Integration of *Equation 23* yields

$$\xi\kappa\int_0^{\varphi}\frac{d\varphi}{\sqrt{1-\kappa^2\sin^2(\varphi)}} = \int_0^{z} \mathrm{dz} \qquad \text{or} \qquad \xi\kappa F\left(\sin^{-1}(\varphi)\,|\,\kappa^2\right) = z\,, \tag{24}$$

where $F\left(\sin^{-1}(\varphi)\,|\,\kappa^2\right)$ is an incomplete elliptic integral of the first kind. Because one quarter of the pitch length corresponds to $\varphi = \pi/2$, we can say

$$P = 4\xi\kappa F\left(\sin^{-1}(\pi/2)\,|\,\kappa^2\right) = 4\xi\kappa K\left(\kappa^2\right), \tag{25}$$

where $K\left(\kappa^2\right)$ is a complete elliptic integral of the first kind, and P is the pitch of the distorted helix. This relation gives us the pitch in terms of κ, which can be thought of as a constant for a given electric field that has to do with the unwinding of the CLC helix.

The only thing left to do, then, is solve for κ. This is made easier by the knowledge that κ will have a value that satisfies the MFE condition for the distorted CLC helix, averaged over one pitch length (since the system always tends toward MFE). It is important to minimize the average free energy over an entire pitch length so that you get an overall minimum, and not just a value of κ that minimizes the energy in some parts of the distorted helix but not others. This average can be found by integrating the

energy per unit volume, *Equation 19*, over an entire pitch length and dividing both sides of this function by the pitch. This step yields

$$\left\langle F_V \right\rangle = \frac{\varepsilon_0 \Delta\chi_e E^2}{2P} \int_0^P \left[\xi^2 \left(\varphi' - q_0 \right)^2 - \sin^2\left(\varphi\right) \right] dz \,, \tag{26}$$

where $\left\langle F_V \right\rangle$ is the average free energy per unit volume. Before minimizing this function, it is useful to rewrite it by changing the integration variable from z to φ, and plugging in the expressions for φ', obtained in *Equation 23*, and the pitch, obtained in *Equation 25*. Doing so yields

$$\left\langle F_V \right\rangle = \frac{\varepsilon_0 \Delta\chi_e E^2}{2\xi\kappa K\left(\kappa^2\right)} \int_0^{\pi/2} \left[\frac{\xi^2 \left(\frac{1}{\xi\kappa} \sqrt{1-\kappa^2 \sin^2\left(\varphi\right)} - q_0 \right)^2 - \sin^2\left(\varphi\right)}{\frac{1}{\xi\kappa} \sqrt{1-\kappa^2 \sin^2\left(\varphi\right)}} \right] d\varphi \,. \tag{27}$$

Rewriting this expression in terms of complete elliptic integrals yields

$$\left\langle F_V \right\rangle = \frac{\varepsilon_0 \Delta\chi_e E^2}{2} \xi^2 {q_0}^2 \left[1 - \frac{\pi}{\xi q_0 \kappa K\left(\kappa^2\right)} - \frac{1}{\xi^2 \kappa^2 {q_0}^2} \left(1 - 2\frac{E\left(\kappa^2\right)}{K\left(\kappa^2\right)} \right) \right], \tag{28}$$

where $E\left(\kappa^2\right)$ is a complete elliptic integral of the second kind, equal to

$$E\left(\kappa^2\right) = \int_0^{\pi/2} \sqrt{1-\kappa^2 \sin^2\left(\varphi\right)}\, d\varphi \,. \tag{29}$$

The minimum of this function can be found by taking its derivative with respect to κ and setting it equal to zero. This process is made easier by noting that

$$\frac{d}{d\kappa}\left(\frac{E\left(\kappa^2\right)}{\kappa} \right) = -\frac{K\left(\kappa^2\right)}{\kappa^2} \tag{30}$$

and that it is not necessary to evaluate the derivative $\frac{d}{d\kappa}\left(\frac{1}{\kappa K\left(\kappa^2\right)} \right)$ because it is a common factor in all terms. From this work, we obtain an expression that κ must satisfy in order to achieve MFE:

$$\frac{E\left(\kappa^2\right)}{\kappa} = \frac{\pi}{2}\xi q_0 . \tag{31}$$

This equation can be further refined by plugging in the expressions for the pitch, *Equation 25*, and the equilibrium pitch, *Equation 11*. After doing so, we finally obtain a relationship between the distorted pitch and the equilibrium pitch

$$\frac{P}{P_0} = \left(\frac{2}{\pi}\right)^2 E\left(\kappa^2\right)K\left(\kappa^2\right). \tag{32}$$

As the result of our minimization of the free energy of a CLC system, *Equations 31* and *32* can be used to determine how the helix changes for a wide range of electric fields. We can tell that when $\kappa^2 = 0$, $E(0) = K(0) = \frac{\pi}{2}$, and therefore $\frac{P}{P_0} = 1$. This means that the helix is undistorted, or that there is zero electric field. The other extreme of *Equation 32* occurs when κ approaches 1; as this happens, $E(1) \to 1$ and $K(1) \to \infty$, which consequently means that $\frac{P}{P_0} \to \infty$. This corresponds to a the helix unwinding transition, where the length of the distorted pitch approaches infinity, at which point, the strength of the electric field is great enough to turn the CLC structure into a nematic LC one. Plugging this condition into *Equation 31*, we obtain the critical value of ξ that occurs when the helix unwinds

$$\frac{E(1)}{1} = \frac{\pi}{2}\xi_c q_0 \qquad \text{or} \qquad \xi_c = \frac{2}{\pi q_0}, \tag{33}$$

where ξ_c is the value of ξ when the helix unwinds. This can be used, in conjunction with *Equations 10, 11,* and *21* to find the critical strength of the electric field, E_c, that unwinds the CLC helix

$$E_c = \frac{\pi^2}{P_0}\sqrt{\frac{K_2}{\varepsilon_0 \Delta\chi_e}} . \tag{34}$$

This expression can be rewritten in terms of intensity of the laser, instead of the electric field, as follows

$$I_c = \frac{\pi^4}{P_0^2}\frac{K_2}{\eta}. \tag{35}$$

This is a useful function because it will allow us to determine what intensity of light we will need to use to effect a significant change in the bulk of the CLC. This analysis can be continued further by combining *Equations 21, 31,* and *34* to yield the ratio between the electric field and the critical electric field

$$\frac{E}{E_c} = \frac{\kappa}{E\left(\kappa^2\right)}. \tag{36}$$

This evaluation sheds light on one of the ways laser emission can change the chirality of the CLC sample. By plotting *Equation 36* against *Equation 32,* we can evaluate how the pitch of the sample varies as the electric field increases. As you can see from *Figure 3*, the pitch of the sample does not change very much as the electric field increases until the ratio of electric field to its critical value exceeds about 0.6. After this point though, the deformation to the helix becomes substantially larger with each step towards the critical electric field.

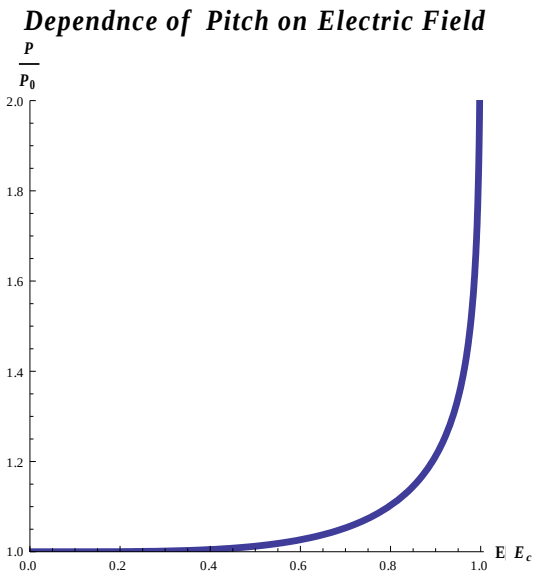

Figure 3: Helical pitch deformation as a function of electric field strength.

The reason we are interested in changing the pitch of the sample lies in the theory behind the photonic band gap (PBG) of CLCs. The band gap phenomenon arises because of interference and diffraction effects that take place as a light wave propagates through the CLC helix. [8] This happens because the CLC helix consists of a large number of thin anisotropic layers, whose refractive indicies rotate through successive layers by an angle φ (this is the result of the definition of the CLC structure and the anisotropy of the LC molecules). This leads to reflections from the boundaries between each of the layers. To model this behavior quantitatively, we can assume that the

CLC helix points in the *z* direction, that the director rotates with respect to the previous layer by the angle $\varphi = q_0 z$ from its initial position along the x axis (*Figure 4*) throughout the material.

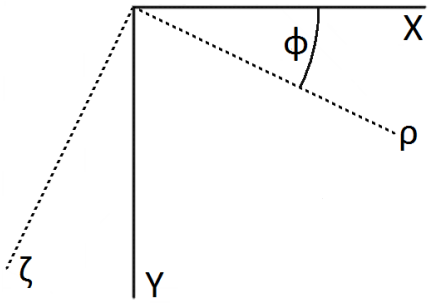

Figure 4: Coordinate system representing successive layers in a CLC sample.

The permittivity of the material can be described at any point along *z* by using rotation matrices to describe its characteristics at rotations away from the initial *x* and *y* axes. Using this method, we obtain

$$\vec{\varepsilon} = \begin{bmatrix} \cos q_0 z & -\sin q_0 z \\ \sin q_0 z & \cos q_0 z \end{bmatrix} \begin{bmatrix} \varepsilon_{\parallel} & 0 \\ 0 & \varepsilon_{\perp} \end{bmatrix} \begin{bmatrix} \cos q_0 z & \sin q_0 z \\ -\sin q_0 z & \cos q_0 z \end{bmatrix} = \begin{bmatrix} \varepsilon_{avg} + \alpha \cos 2q_0 z & \alpha \sin 2q_0 z \\ \alpha \sin 2q_0 z & \varepsilon_{avg} - \alpha \cos 2q_0 z \end{bmatrix}, \quad (38)$$

where $\vec{\varepsilon}$ is the permittivity of a any layer in the sample, $\varepsilon_{\parallel}$ are $\varepsilon_{\perp}$ the permittivities of the LC molecules parallel and perpendicular to their long axis, $\varepsilon_{avg} = (\varepsilon_{\parallel} + \varepsilon_{\perp})/2$ is the average permittivity of the LC molecule, and $\alpha = (\varepsilon_{\parallel} - \varepsilon_{\perp})/2$. This can be used in the wave equation for propagation along the *z* axis (derived from Maxwell's equations)

$$\frac{\delta^2 \vec{E}}{\delta z^2} = -\frac{\omega^2}{c^2} \vec{\varepsilon} \vec{E}, \quad (39)$$

where *c* is the speed of light, and ω is the angular frequency of the light wave. We define the right (E') and left (E'') circular light components as

$$\begin{aligned} E' &= (E_x + iE_y)/\sqrt{2} \\ E'' &= (E_x - iE_y)/\sqrt{2} \end{aligned}, \quad (40)$$

where E_x and E_y are the *x* and *y* components of each wave. Combining *Equations 38, 39,* and *40* yields

$$\begin{bmatrix} \frac{\delta^2 E'}{\delta z^2} \\ \frac{\delta^2 E''}{\delta z^2} \end{bmatrix} = -\frac{\omega^2}{c^2} \begin{bmatrix} \varepsilon_{avg} & \alpha e^{2iq_0 z} \\ \alpha e^{-2iq_0 z} & \varepsilon_{avg} \end{bmatrix} \begin{bmatrix} E' \\ E'' \end{bmatrix}, \quad (41)$$

which we can reasonably assume has a solution in the form of a traveling wave

$$u = \begin{bmatrix} A' e^{i(k+q_0)z} \\ A'' e^{i(k-q_0)z} \end{bmatrix}, \tag{42}$$

where A' and A'' are amplitude constants, and k is the wavevector of the light travelling through the sample. Combining *Equations 41* and *42*, we get

$$\begin{bmatrix} (k+q_0)^2 - {K_m}^2 & -\alpha K^2 \\ \alpha K^2 & (k-q_0)^2 - {K_m}^2 \end{bmatrix} \begin{bmatrix} A' \\ A'' \end{bmatrix} = 0, \tag{43}$$

where $K = 2\pi/\lambda$ and $K_m = 2\pi m/\lambda$ are wavevector constants and λ is the wavelength of the light beam in a vacuum. Physically significant solutions to *Equation 43* can be found by taking the determinant of its 2x2 matrix and solving for both roots of k yields

$$k_2, k_1 = \sqrt{{K_m}^2 + q^2 \pm \sqrt{4{K_m}^2 q^2 + \alpha^2 K^4}} \,. \tag{44}$$

Plugging each solution back into *Equation 43* and solving for the ratios A'/A'' and A''/A', we obtain

$$\frac{A'}{A''} = \frac{\alpha K^2}{(k_1+q)^2 - {K_m}^2} \tag{45}$$

$$\frac{A''}{A'} = \frac{\alpha K^2}{(k_2-q)^2 - {K_m}^2}. \tag{46}$$

These relations can be used in conjunction with *Equations 42* and *44* to solve for two specific solutions to the traveling wave equation

$$\vec{u}_1 = \begin{bmatrix} e^{iK_1 z} \\ d e^{i(K_1 - 2q_0)z} \end{bmatrix} \tag{47}$$

$$\vec{u}_2 = \begin{bmatrix} f e^{i(K_2 + 2q_0)z} \\ e^{iK_2 z} \end{bmatrix} \tag{48}$$

where

$$K_1 = k_1 + q = q + \sqrt{{K_m}^2 + q^2 - \sqrt{4{K_m}^2 q^2 + \alpha^2 K^4}} \tag{49}$$

$$K_2 = k_2 - q = -q + \sqrt{{K_m}^2 + q^2 + \sqrt{4{K_m}^2 q^2 + \alpha^2 K^4}} \tag{50}$$

$$d = \frac{{K_1}^2 - {K_m}^2}{\alpha K^2} \quad \text{and} \quad f = \frac{{K_2}^2 - {K_m}^2}{\alpha K^2} \ . \tag{51}$$

From these equations we can tell that the optical rotation per unit length along the helix will be $p_{rot} = (K_1 - K_2)/2$ radians. Furthermore, because the light's rotation per pitch length is small compared to pi, we can say

$$p_{rot} = \frac{K_1 - K_2}{2} = -\frac{{K_m}^2 - {q_0}^2 - \sqrt{\left({K_m}^2 - {q_0}^2\right)^2 - \alpha^2 K^4}}{4q_0} . \tag{52}$$

This rotation becomes imaginary whenever $\left({K_m}^2 - {q_0}^2\right)^2 < \alpha^2 K^4$, so we can say that this condition gives us the region of wavelengths that will be reflected to form the PBG. This happens whenever

$$-\alpha K^2 \le {K_m}^2 - {q_0}^2 \le \alpha K^2 . \tag{53}$$

These conditions can be rewritten with previously defined variables in the form of a wavelength interval

$$n_\perp P \le \lambda \le n_\parallel P \ , \tag{54}$$

where $n_\parallel$ and $n_\perp$ are the refractive indices of the LC molecules parallel and perpendicular to their long axis. This equation can be rewritten in a more useful way by solving for the wavelength that corresponds to the center of the PBG, λ_c, and the width of the PBG, $\Delta\lambda$

$$\lambda_c = P\frac{(n_\parallel + n_\perp)}{2} \tag{55}$$

$$\Delta\lambda = P(n_\parallel - n_\perp). \tag{56}$$

These last few expressions are very valuable because they tell us the wavelengths of light that a particular CLC sample will reflect (given the appropriate information). Furthermore, *Equations 55* and *56*

can be combined in a way that allows you to solve for the pitch or either of the indices of refraction, provided information is available about the characteristics of the PBG and either the pitch or one of the indices of refraction. These relations can be expressed as follows

$$\begin{aligned} 2Pn_{\parallel} &= 2\lambda_c + \Delta\lambda \\ 2Pn_{\perp} &= 2\lambda_c - \Delta\lambda \end{aligned}. \tag{57}$$

This knowledge about the characteristics of the PBG leads to another way laser emission can change the chirality of the sample. The reorientation of the director at the surface, and the resulting shift in the easy axis of the sample, will either twist or untwist the helix of the sample, depending on whether the reorientation is in the opposite or same direction as the helix (respectively), kind of like twisting a ribbon at one end while the other end remains fixed. This process is much simpler than the previous helix unwinding mechanism, and, given the pitch and thickness of the sample, we can determine how such reorientations would alter the length of the pitch. We know, from our previous analysis, that the equilibrium pitch of the sample can be expressed as the total thickness of the sample, P_0, divided the total number of pitches in that thickness at equilibrium, N_0

$$P_0 = \frac{L}{N_0}. \tag{58}$$

It follows from this that rotating the sample's director on one side by an angle Φ_T will give a new number of pitch lengths, N, such that

$$N = N_0 + \frac{\Phi_T}{2\pi} = \frac{L}{P_0} + \frac{\Phi_T}{2\pi}. \tag{59}$$

Using *Equations 58* and *59*, it is straight forward to show that the new pitch of the sample, P, is

$$P = \frac{P_0}{1 \pm \frac{\Phi_T}{2\pi}\frac{P_0}{L}}. \tag{60}$$

If we define the change in pitch, ΔP, as $\Delta P = P - P_0$, we can then rewrite *Equation 60* in terms of this

change in pitch,

$$\Delta P = \frac{\mp \frac{\Phi_T}{2\pi} \frac{P_0^{\,2}}{L}}{1 \pm \frac{\Phi_T}{2\pi} \frac{P_0}{L}}. \tag{61}$$

This function represents a second way that we can quantify the change in pitch of our sample due to rotations of the surface director. The utility of this function doesn't end here though; by plugging *Equations 55* and *56* into *Equation 61* and solving for the rotation of the director, we discover a crucial relationship between the characteristics of the PBG and changes in the structure of the sample,

$$\Phi_T = 2\pi n L \frac{\Delta\lambda}{\lambda_c}. \tag{62}$$

where n is the average index of refraction $n = \left(n_{\parallel} + n_{\perp}\right)/2$.

As will be shown in the next section, this theory can then used to design experiments that investigate the dynamics of the interactions between polarized laser emission and the structure of CLC samples. Through data collection and analysis, the models developed in this section can also be tested against experimental findings, and evaluated for their veracity. To do this, experiments will be conducted that utilize Stokes Polarimetry to track changes in the structure of CLC samples and that measure the PBG with UV-Vis spectroscopy.

Experimental Method

To make the CLC used for sample preparation, the nematic LC E7 (Licristal) was mixed with the chiral doping agent CB15 (Licristal) in a ratio of 16:9, and then doped with 0.6 percent Methyl Red (MR) azo-dye (Sigma Aldrich). (The uncertainty in the ratios of E7 to CB15 and the percentage concentration of dye were very low because the weights of each were measured out to within 0.001 grams of their required masses.) These parameters were chosen because previous research has determined that the PBG for this mixture lies between 615 and 665 nm, and produces an equilibrium CLC pitch length of

approximately 380 nm. [9] This mixture was then used to fill a prepared cell, which was fabricated earlier with a coating of rubbed polyimide (PI) on both sides of the interior surface of the cell. The thickness of the cells was approximately 1.5 µm, because of plastic spacers inserted between the glass slides during preparation. The sample preparation process is discussed in full in *Appendix A*.

The experimental setup used to measure the 2nd Stokes parameter (2SP) and 3rd Stokes parameters (3SP) of a CLC sample under exposure to Argon laser emission is depicted in *Figure 5*. The Stokes parameters are important because they can tell us about what is going on within the sample before, during, and after irradiation. The 2SP tells us the difference between the intensities of light polarized along the *x* and *y* directions of a coordinate system rotated by +45 degrees. My measurements are scaled in such a way as to give the Stokes parameters as a ratio between the measured signal and the maximum signal for each direction in question. This means that light polarized entirely along the x direction would produce a 2nd Stokes parameter of +1, light entirely along the y direction would give -1, and completely vertically polarized light would give a reading of 0 (this arises because the Stokes parameter is calculated as a difference between the x and y intensities). This Stokes parameter can

Figure 5: Experimental setup for conducting Stokes Polarimetry.

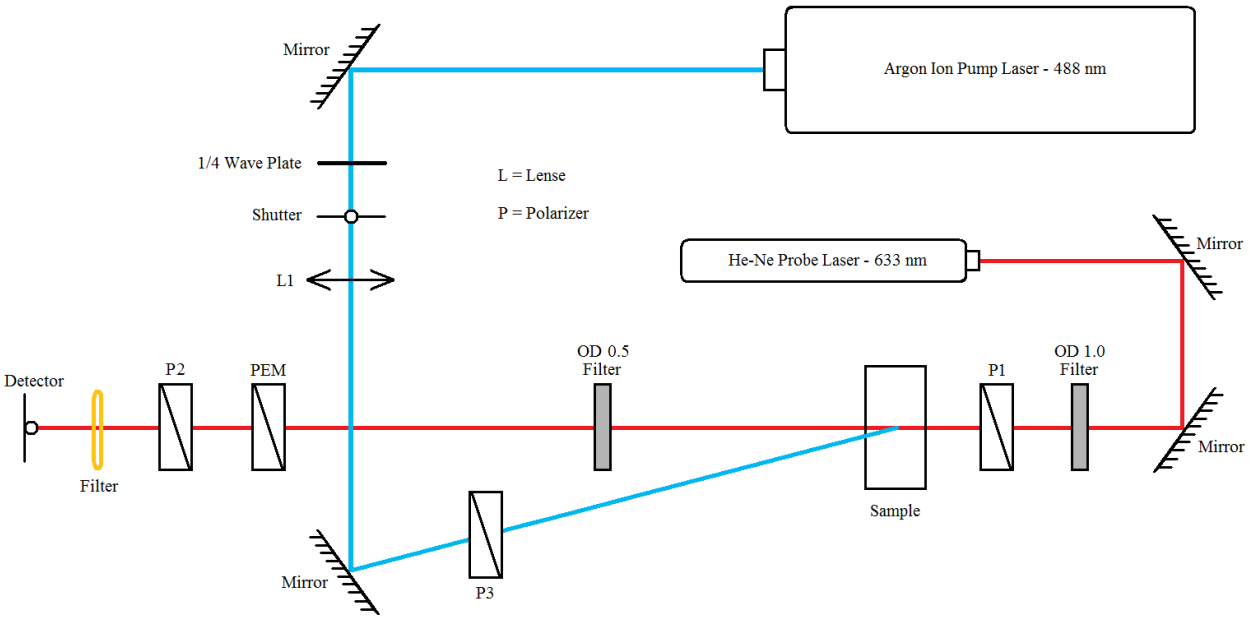

therefore tell me about the orientation of the major axis of the ellipse traced out by the optical field of the probe light coming out of the sample. This in turn informs me about any possible twisting that may be occurring as a result of the pump beam.

The 3SP is very similar to the 2SP, except it measures the difference in intensities between left and right circularly polarized light. Accordingly, I have also scaled the 3SP so that +1 corresponds to purely right handed light, -1 corresponds to purely left handed light, and 0 corresponds to linearly polarized light. This quantity can tell us about how circular the probe light is after passing through the sample, which informs us about the chiral structure of the liquid crystal sample itself. By recording both of the 2SP and the 3SP simultaneously, I can measure real time changes in characteristics like the orientation of the director on the irradiated surface, and the ellipticity (and the major axis of this ellipse) of the light exiting the sample.

In this experimental setup, the Argon ion laser, which has a wavelength of 488 nm, produces what is called the pump beam. This beam creates the optical field that induces reorientations in the sample. It passes through a system of mirrors that direct it towards the sample, a shutter to block and unblock the beam, a quarter wave plate which can be adjusted to help control the intensity of the beam, lens 1 which serves to focus the beam on the sample, and polarizer 3 which can be adjusted to control the polarization of the pump beam that hits the sample. All of my tests have been executed with polarizer 3 set at ±45 degrees relative to the vertical. This angle was chosen because it should cause the maximum amount of reorientation, since the surface anchoring in all the samples is vertical.

Changes in the sample's helical structure and easy axis are measured by sending what is called a probe beam through the sample, and measuring the changes in its state with a Photo-Elastic Modulator (PEM). In this experiment, a He-Ne laser with a wavelength of 633 nm will be used as a probe beam. The probe beam passes through polarizer 1 which sets the polarization that goes through the sample (this should be vertical because the rubbing, and thus the director in the sample is vertical), the sample itself

which changes the polarization state of the beam continuously as the structure of the sample changes, and OD 1.0 and 0.5 filters which bring the intensity of the probe down to levels that the Lock-In amplifiers can more easily process, the PEM which modulates the probe beam so that the detector can read its characteristics, polarizer 2 which is crossed with polarizer 1 to allow for the measurement of the appropriate Stokes parameters, a yellow-orange filter to screen out any trace light from the pump beam, and finally a detector which measures the intensity of the probe beam.

The output from the detector is run through two SR510 Lock-In Amplifiers, one for the 1st and one for the 2nd harmonics, which correspond to the 3rd and 2nd Stokes parameters, respectively. These Lock-In amplifiers take the ratio of signal they are measuring to the RMS voltage output of the detector to eliminate intensity dependent variations in our measurements. To make it possible to measure larger signals and improve the signal to noise ratio, an operational amplifier, whose circuit diagram is depicted in *Figure 6*, was added to amplify the RMS voltage. This works by decreasing the aforementioned ratio so that more sensitive measurements may be taken. Data about this ratio from each Lock-In is then fed into a LabVIEW program which compiles our data and runs the amplifiers. During experiments, the

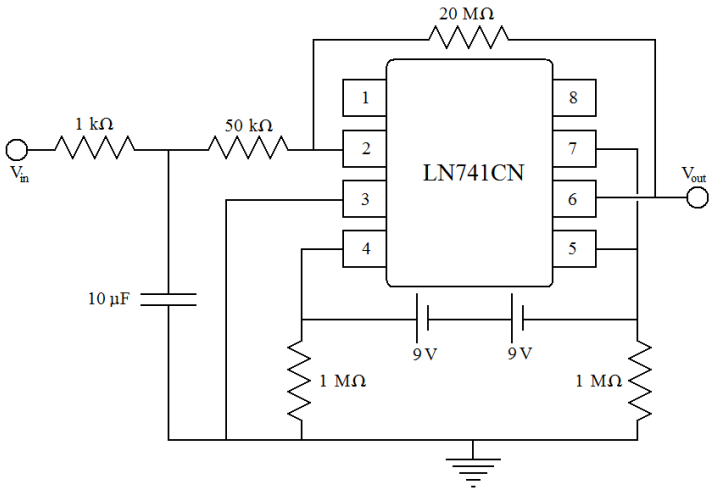

Figure 6: Circuit diagram of operational amplifier and low pass filter used in the amplification of RMS signal voltage.

sample is held in a heat stage which holds the sample at a desired temperature. Most of the experiments were run at 20 °C, and irradiation times varied for different samples, as did the pump

intensities. Before and after irradiation, data was taken on each Stokes parameter until a steady state was reached so that the only changes that occurred were the result of the pump beam and not, for example, the sample acclimating to the 20 °C temperature controller.

To determine the PBG of the sample, the absorbance of a region of CLC was measured both before and after irradiation by the pump beam, on both side of the sample. Absorbance is measured because light traveling through the sample with a wavelength in the PBG is either absorbed or reflected back, while all other wavelengths are transmitted through. This measurement cannot be done on a sample while it is being exposed to laser radiation because the laser light would wash out any spectra, and it is therefore conducted immediately before and after data collection is complete for the Stokes parameters. The absorbance is measured using an Ocean Optics UV-Vis Spectrometer, laid out as depicted in *Figure 7*. The lenses come from 3D movie glasses, which produce left or right circularly polarized light depending on whether the signal light passes through the left or right lens. These glasses were used to measure the absorbance of the left and then the right handed light signals. These measurements give the PBG of the sample, however changes in the orientation of the sample while measuring its spectra, or between laser exposures, can change the readout for the PBG of the sample. It is therefore necessary to ensure that the alignment of the sample in the spectrometer layout remains the same for every trial.

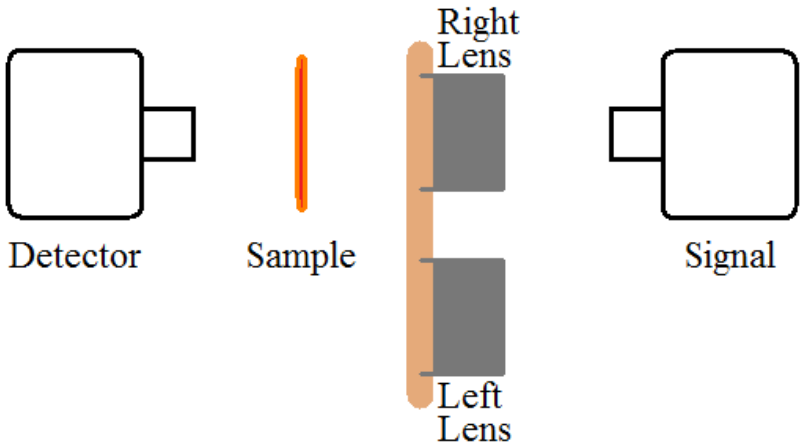

Figure 7: Setup for measuring a sample's absorbance of right handed light.

In order to further track changes in the structure and the overall appearance of samples, pictures were taken of the irradiated region before and after each test under a crossed microscope. This will help to track the possible formation of any focal conic regions in the sample, or other structural changes induced during the course of testing. Also, for the final run of experiments, digital camera pictures of the sample were taken through circularly polarized lenses to track changes in the macroscopic appearance of the PBG throughout testing.

Experimental Results and Analysis

All of the data collected during my testing came from samples filled with the LC mixture described at the beginning of the *Experimental Methods* section, and had interior surfaces coated in polyimide which were rubbed along the long axis of the cell. The first set of data that was collected came from a prefabricated Instec cell that was 25 μm thick. This sample was irradiated for 1000 seconds at room temperature, with a 30 mW pump intensity oriented at +45° to the vertical. This test resulted in the formation of numerous little dark spots all throughout the irradiated region, which congealed over time into a large focal conic region that spanned the entire irradiated area. The progression of this process can be seen in *Figures 8a-8d* on the following page. This focal conic texture did not go away with time, and was present only at the irradiated surface within the irradiated region.

It is believed that the pump beam causes a trans-cis isomerization in the methyl red (MR) dye molecules, and that some of these cis MR molecules subsequently adsorb to the inside surface of sample at the irradiation site. In this process, the N=N bond of the cis MR molecule gets adsorbed to the surface, and the two benzene rings stick straight out into the bulk of the LC contained within the sample. The adsorbtion of more and more of these cis MR molecules throughout the irradiation process eventually makes the normal grandjene structure less energetically favorable because the adsorbed MR molecules hinder LC alignment along the surface, and instead encourage LC alignment along the MR

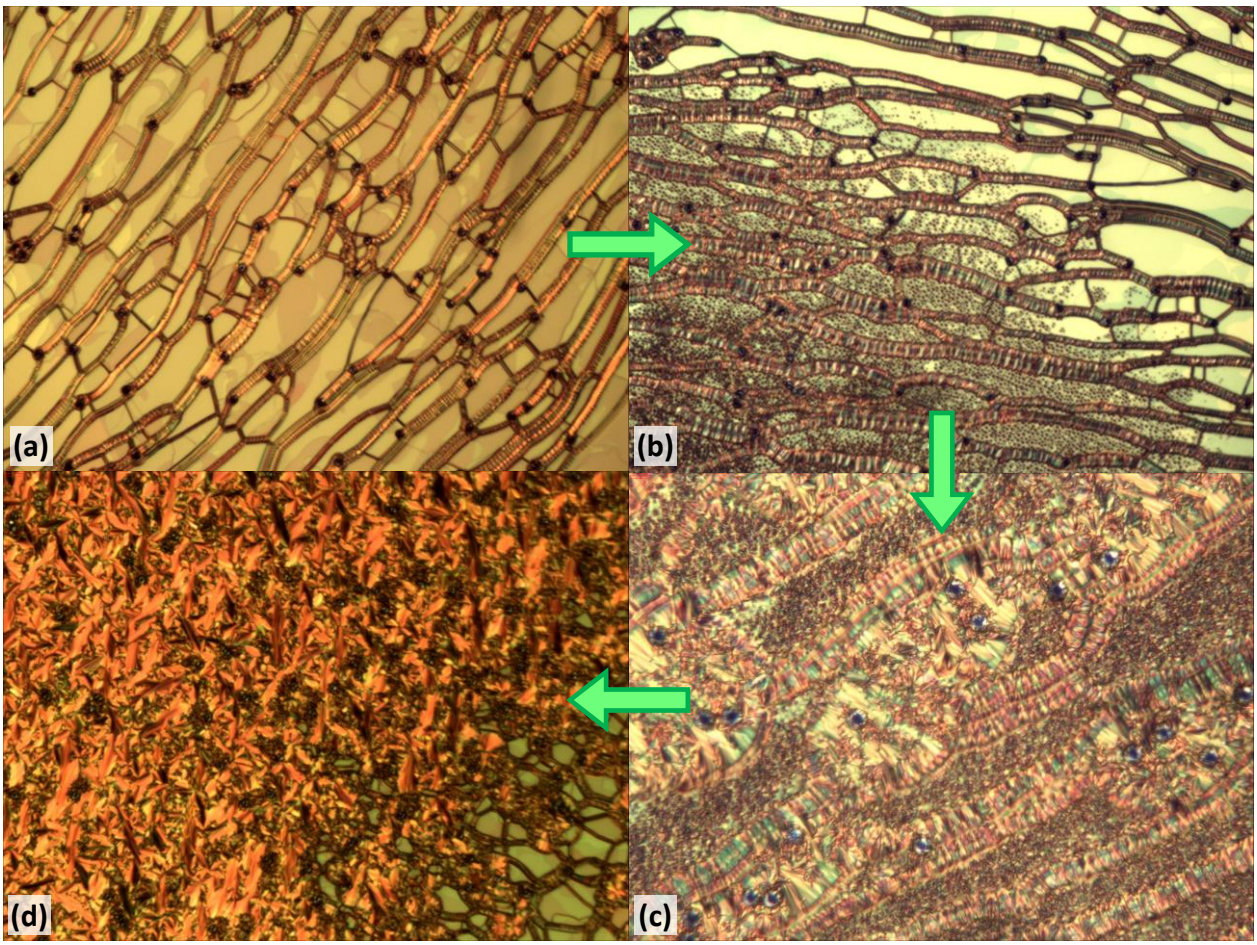

Figure 8: Microscopic pictures of tested Instec sample at (a) initial condition, (b) immediately after testing, at the edge of the irradiated region, (c) immediately after testing, at the center of the irradiated region, and (d) one week after testing, at the edge of the irradiated region.

molecules sticking out of the inside surface of the sample. Essentially what happens is that the helix of the CLC turns on its side and destroys the original grandjene structure of the sample. This new focal conic texture would at least partially destroy any PBG, and through the increased scattering and absorbtion of light, increase the absorbance of the sample. This result was found in the absorbance data that was collected for both the left and right handed light, before and after testing, as seen in *Figure 9* on the following page. In this figure, the PBG is the absorbtion peak which initially spans the right handed spectrum from approximately 625 nm to 675 nm.

Because of the formation of focal conic structure, the sample begins to absorb more left and right handed light, and the definition of the PBG begins to decrease as the increasing absorbtion

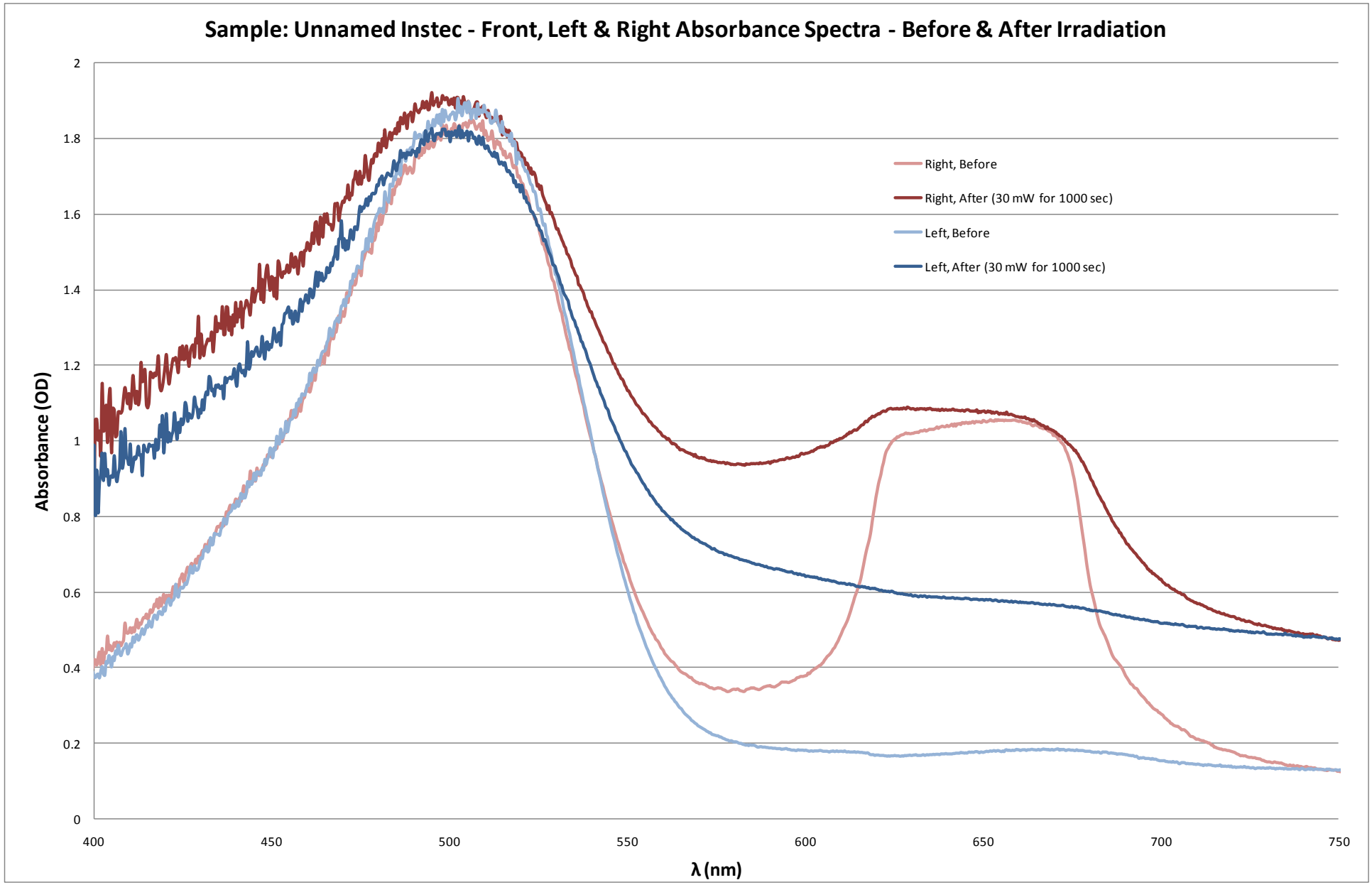

Figure 9: Absorbance spectra profile of the front side of the Instec sample for initial and final conditions, as measured with right and left handed light. The PBG, centered around 650 nm for right handed light, begins to lose definition with respect to left handed light as a result of the formation of focal conic structure. It is clear from the final condition that, overall, the sample absorbs a much greater amount of both left and right handed light.

and scattering from the focal conic structure begins to become more prominent. This phenomenon is very interesting and will no doubt need to be a factor in future analysis, but ultimately, because the focal conic structure does not disappear, the formation of such large focal conic regions inhibits our ability to measure changes in the shape, width, or location of the PBG (it also prevents further testing from being carried out on this particular sample). To minimize this problem, tests after this point were conducted with the heat stage on and set to 20 $^{\circ}$C to minimize thermal excitations of the MR molecules and to keep the sample well below the clearing point (the melting point of the CLC, when it becomes isotropic). Furthermore, in an attempt to determine an intensity threshold at which the focal conic structure appears, earlier tests were run with low pump intensities that increased gradually with each successive test. (The Stokes parameter measurements for the test on the Instec sample were not included within this analysis because there were problems in the Stokes Polarimetry setup and calibration that were being worked on at the time of the experiment.)

The next set of tests were run on a sample named “Halitosis”, which was 60.42 μm thick. Each test was conducted with the sample held at 20 $^{\circ}$C and the pump oriented at +45°. There were four tests carried out on this sample: test one had an irradiance of 5 mW and was irradiated for 350 seconds, test two had an irradiance of 10 mW and was irradiated for 250 seconds, test three had an irradiance of 15 mW and was irradiated for 1500 seconds, and test four had an irradiance of 20 mW and was irradiated for 2950 seconds. In each test the sample was irradiated until it reached a steady state, which is why the irradiation times varied. The idea behind this was to allow the maximum amount of change in the director of the sample to take place, this would in turn (hopefully) maximize any twists exerted by the optical field, and therefore maximize any changes in the PBG of the sample.

The microscopic images of the sample from tests one through four can be found in *Figure 10a-10d*. The changes in the color of the sample are inconsequential and result from changes in the sample’s orientation and the white balance of the digital camera. After tests one and two, there are no

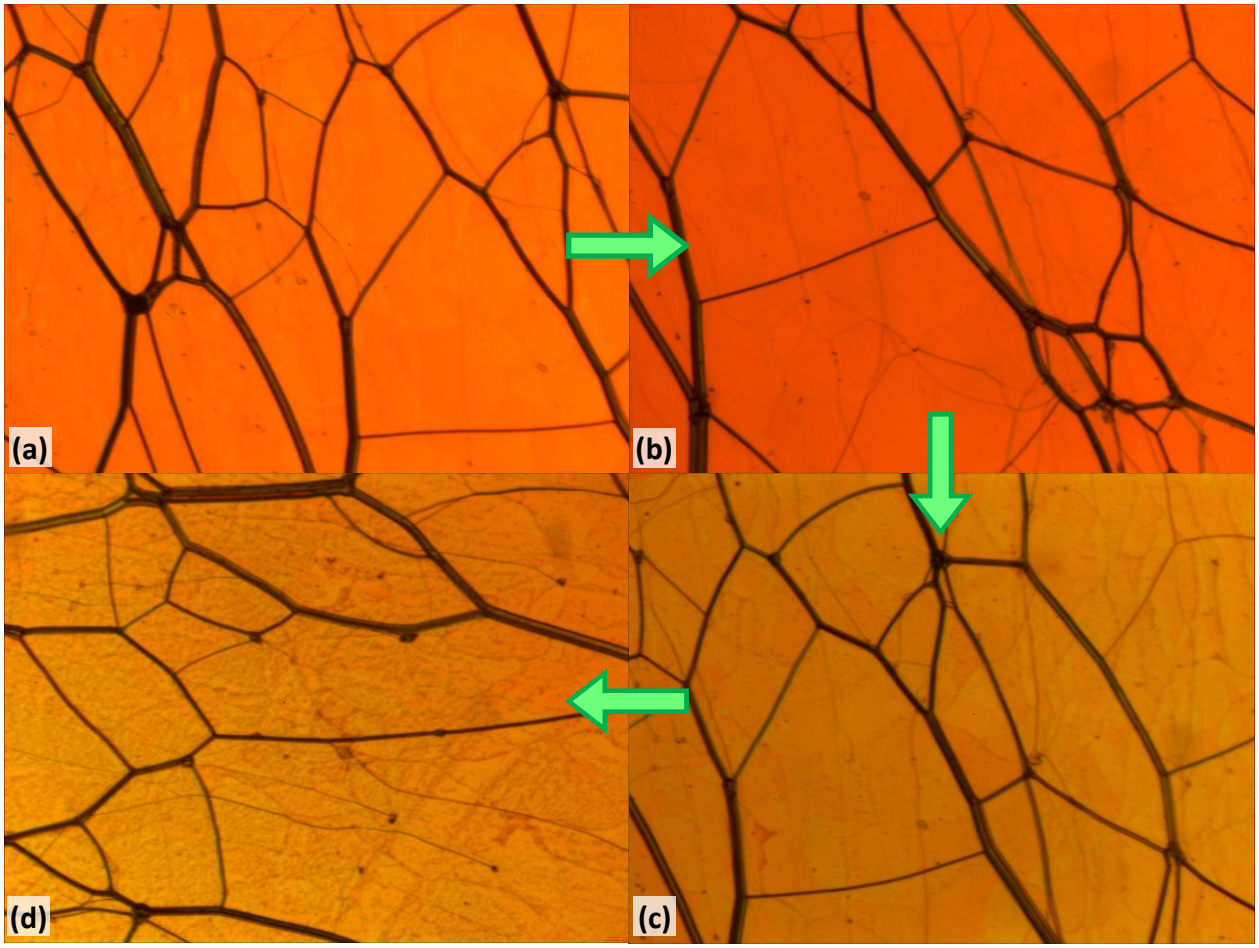

Figure 10: Microscopic pictures of sample "Halitosis" after (a) Test 1, (b) Test 2, (c) Test 3, and (d) Test 4. There are no significant changes after Test 1 or Test 2, but after Test 3 the irradiated region is sparsely covered in very small dark spots, and after Test 4 the spots in the irradiated region become larger and more densely packed.

discernable changes in the overall appearance of the sample, but after test three small spots appear throughout the irradiated region (they are hard to see in the photograph), and after test four the spots become larger and more densely packed. This finding is consistent with the theory that MR is being adsorbed to the inside surface of the irradiated region because, as the sample is irradiated, more MR adsorbs to the inside surface of the cell, and with time more regions begin to flip to the focal conic structure as this becomes more energetically favorable. This theory is further supported by the absorbtion spectra of left and right handed light traveling through the sample. This data is depicted in *Figures 11* and *12*, respectively (shown on the next two pages). *Figures 11* and *12* clearly show an

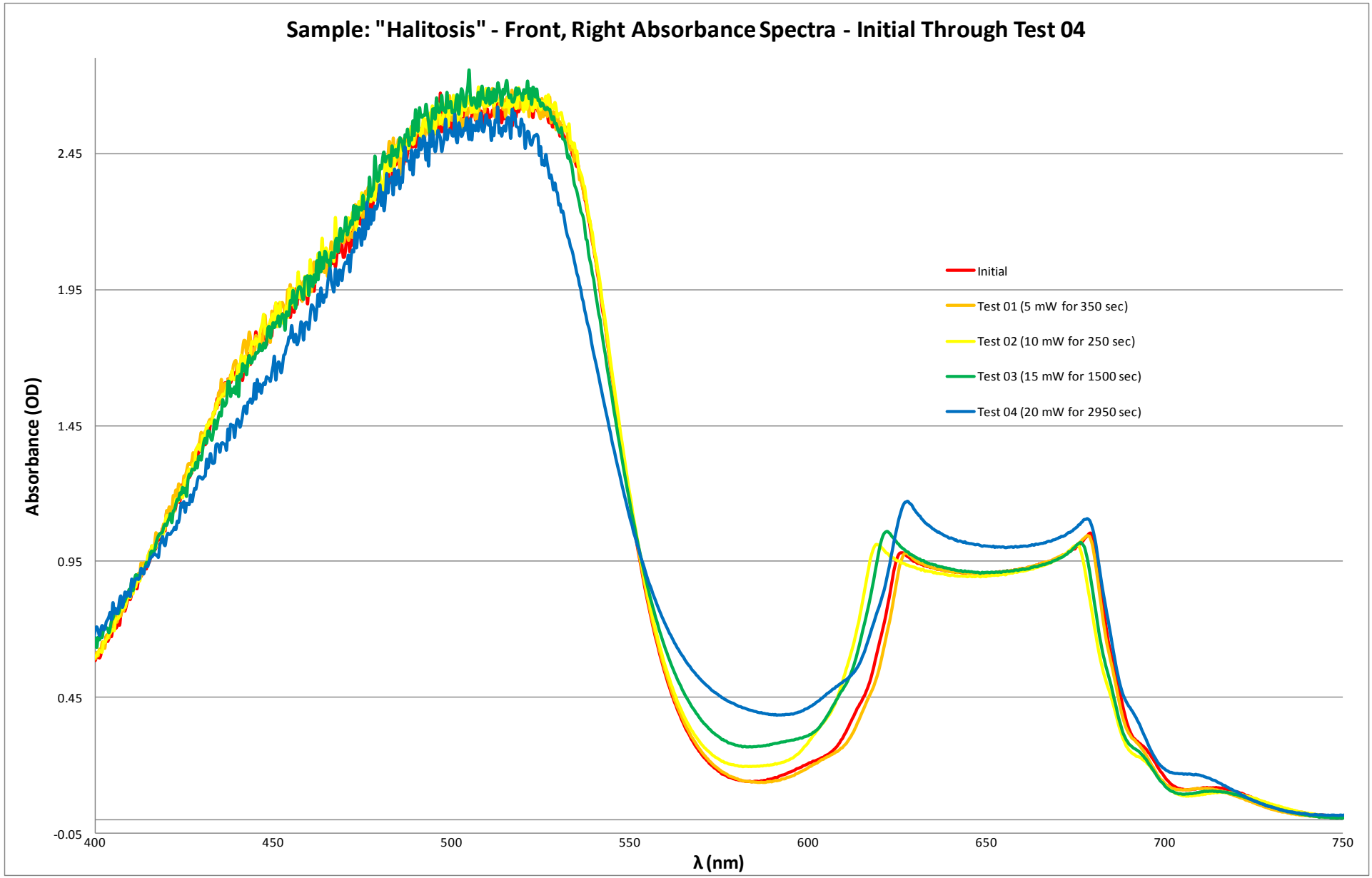

Figure 11: Absorbance spectra profile of the front side of sample "Halitosis" for the initial conditions through Test 4, as measured with right handed light. The PBG is the plateau centered around 650 nm, and it appears to shift to the left at first and then to the right. There is also an absorbtion peak from the trans isomer of methyl red dye, centered around 500 nm, which doesn't change much, and a prevalent increase in absorbtion around 575 nm, which is consistent with the beginnings of the formation of focal conic structures.

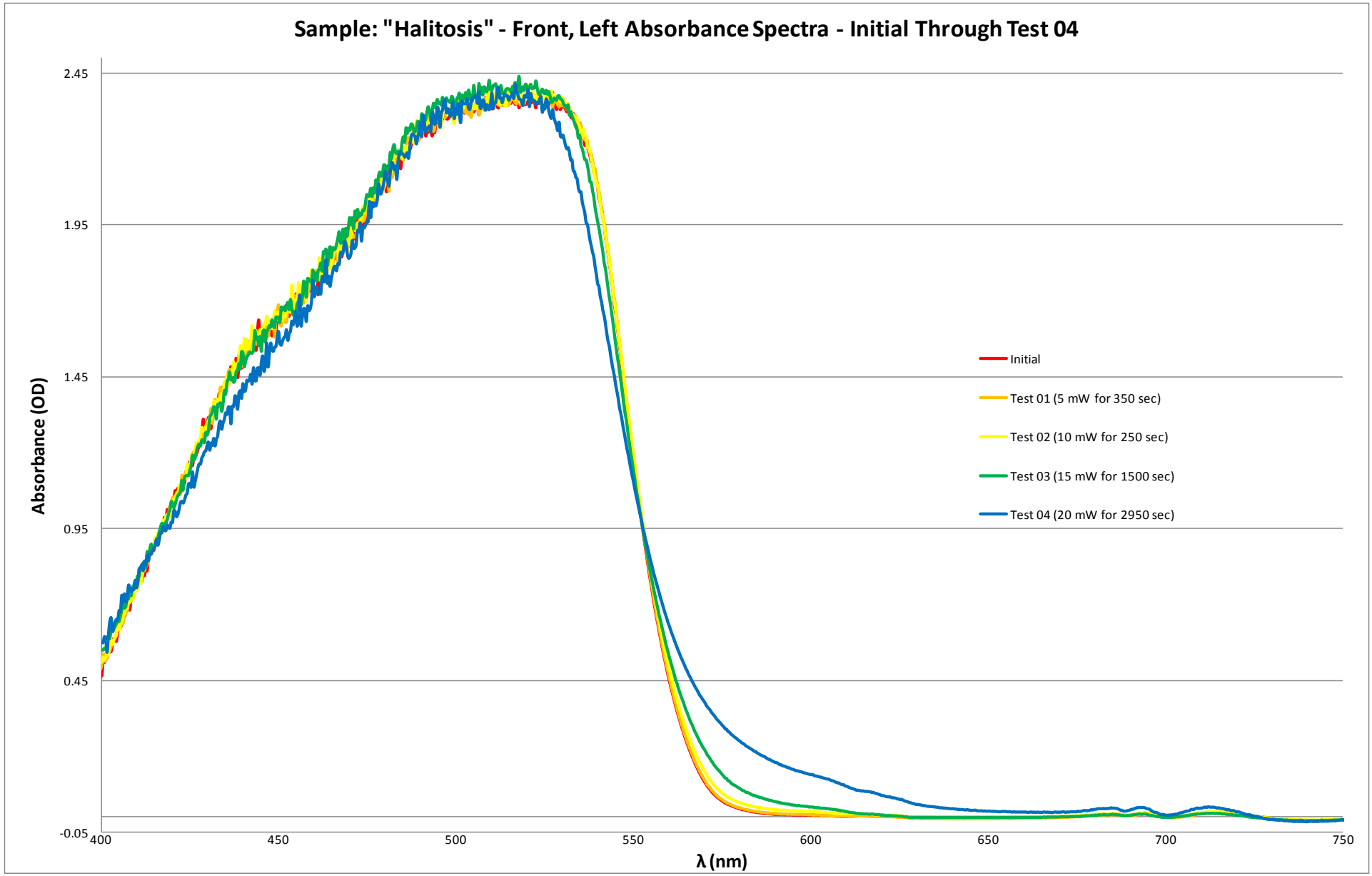

Figure 12: Absorbance spectra profile of the front side of sample "Halitosis" for the initial conditions through Test 4, as measured with left handed light. There is no PBG, but there is still an absorbtion peak from the trans isomer of methyl red dye, centered around 500 nm. There is a prevalent increase in absorbtion around 575 nm, which is consistent with the beginnings of the formation of focal conic structures.

increase in the absorbtion of light around 575 nm for both left and right handed light. This is consistent with the initial stages of the creation of a focal conic structure, because (as we saw in the data from *Figure 9*) the focal conic structure shows high absorbances around this region. Thankfully though, these spots did not absorb enough light to overshadow changes in the PBG of the sample.

As can be seen in *Figure 11*, the PBG shifts to the left a great deal after test two, then appears to gradually shift back to the right, towards its original location. It is possible to see how much of a rotation the tests caused in the director by utilizing the theory developed earlier. Applying *Equation 55* and the knowledge that the pitch length of our sample is 380 nm and the PBG is centered at 652.8 nm, we can calculate that the average index of refraction is equal to 1.72. Next, using *Equation 62* and the fact that the maximum shift in the PBG is equal to 7.04 nm, we can solve for the rotation of the director; doing so gives Φ_T = 10.77 rad. This result is quite large, and outside the range of possible rotations caused by the optical field of the pump beam. The maximum rotation that the pump could have given would have been 45° or 0.785 rad, as this was the orientation of the pump's beam. This result even lies outside the range of possible rotation that MR can have for this pump orientation. From previous studies conducted by other students in Dr. Statman's lab, we know that the pump can cause the MR director to rotate up to 40° or 0.698 rad in standard nematic LC samples when the pump is set at 45°. This result demonstrates that there must be another process causing changes in the PBG of the CLC sample. To make rotations in the director a significant factor in the behavior of the CLC system, thinner samples are needed.

When the optical field of the pump twists the director of a 60.42 μm thick sample, the rotation is distributed across all the pitch lengths that span this thickness, which amounts to 159 pitch lengths for the CLC we are using. To get a more appreciable change in the PBG due to director twisting, we need a much smaller number of pitch lengths. Using *Equation 62* again, it can be calculated that in order to get a 7.04 nm PBG shift from a 20° rotation in the director, a 1.96 μm thick sample is required.

(Unfortunately, the Stokes parameter measurements for the tests on “Halitosis” were not included within this analysis either because there were still prevailing problems in the Stokes Polarimetry setup and calibration that were being resolved at the time of these experiments.)

To draw out these rotation based changes, much thinner and more uniform samples were created. The sample that the final set of tests were run on is called “Lyod” and it was 1.97 µm thick at the center of the sample, where testing was carried out. The irradiation time was changed to 900 seconds for each test conducted on “Lyod” to eliminate the variable irradiation time that occurred previously as a result of waiting for the sample to come to a steady state. This approach eliminated the variable of irradiation time, hopefully making analysis simpler. Also, there were 11 tests run on “Lyod”, each with a pump polarization of -45°, a temperature of 20 °C, and a pump intensity that started at 5 mW and increased by 5 mW for each successive test, ending at 55 mW for test 11.

The microscopic images of “Lyod” at various points throughout testing can be found in *Figure 13a-13d* on the following page, as well as a comparison of irradiated and unirradiated regions after test 10 in *Figure 14a-14b*. To be clear, the alternating light and dark lines shown in *Figure 13a-13d* and *Figure 14b* are phenomena that arise from gradual changes in the thickness of the sample, not something that the testing did to the sample (although testing can affect the boundaries of such lines). These structures appear because there must be a half integer number of pitch lengths in between the edges of the sample. To accommodate this requirement, the pitch length of the sample will change as the sample thickness changes. If, however, the thickness of the sample increases or decreases enough that another half pitch length can fit in or be taken out, the sample will do this instead of continuously increasing or decreasing the pitch length. A diagram of this process is pictured in *Figure 15* on *Page 35*. The only difference between the real thing and my schematic is that where we have to look down into the sample with the microscope (along the thickness of the sample), this schematic shows a cross section of the sample. The numbers on the right indicate the number of half integer pitch lengths that fit

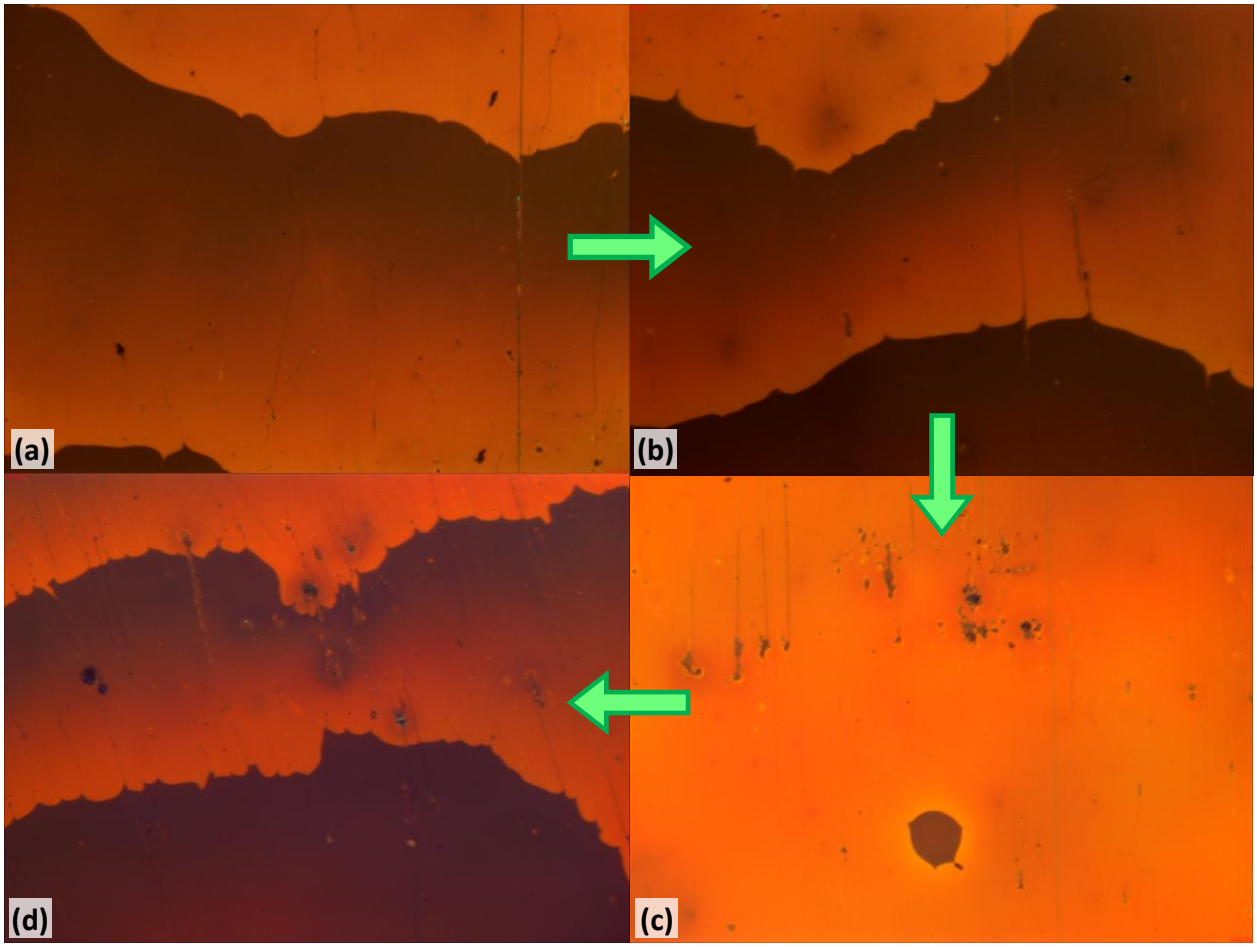

Figure 13: Microscopic pictures of sample "Lyod" after (a) Initial Conditions, (b) Test 03, (c) Test 06, and (d) Test 09. Each successive test shows the formation of more dark patches and disclinations.

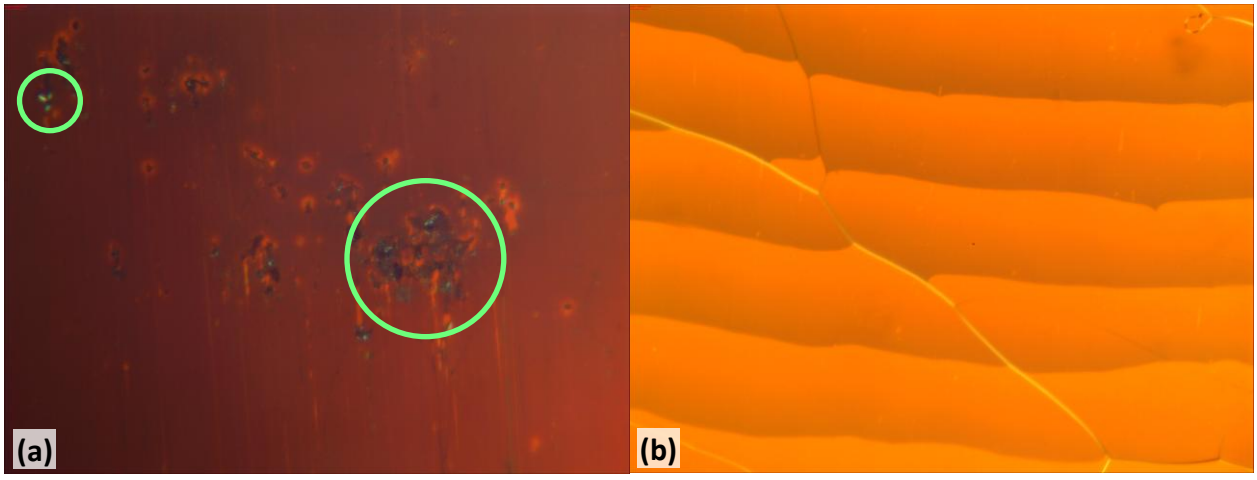

Figure 14: Microscopic pictures of sample "Lyod" after Test 10 in (a) and irradiated region showing the growth of focal conic structures (circled), and (b) an unirradiated region, free of disclinations caused by exposure to pump irradiation. Image (b) does have disclinations caused by the varying thickness of the sample and the filling process though.

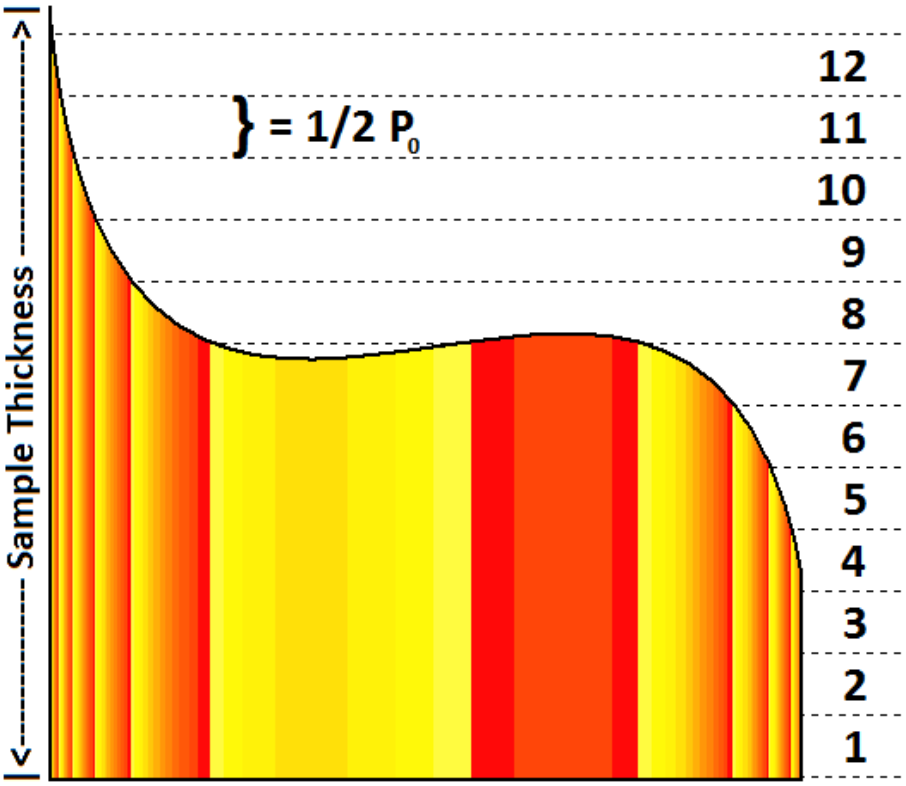

Figure 15: Cross-sectional schematic depicting the process through which the pitch of a CLC sample increases or decreases continuously until another half integer pitch can fit in or be taken out (respectively). The numbers on the right indicate the number of half integer pitch lengths that fit within the sample for a given thickness.

in between the top and bottom of the sample cell, and each different color indicates a slightly different pitch length. This also turns out to be the case for the sample "Lyod" because the different pitch lengths appear as slightly different shades of red, and in the case of the PBG, these varying pitch lengths reflect slightly different wavelengths of light, which gives us the range of wavelengths over which the PBG spans. This type of structure was not as visible in previous samples because of the large number of disclinations that were produced during sample filling (these disclinations look like the veins in *Figure 8a-8d*, *Figure 10a-10d*, and *Figure 14b*), and the variation in sample thickness of the other samples. In the case of the Instec cell, the thickness was extremely uniform because it was machine made, so not many of these pitch flip disclinations appear. In the case of "Halitosis", the thickness was not very uniform at all, so there weren't the distinct lines that appear in the sample "Lyod", where the thickness changes gradually.

The light and dark bands depicted in *Figure 13a-13d* and *Figure 14a-14b* can almost be thought of as the lines on a topographical map, where the least number of these disclinations in any particular region indicates the most uniform sample thickness. It is for this reason that tests on “Lyod” were done at the center of the sample, where these pitch flip disclinations were most spread out (and therefore the thickness of the sample was most uniform).

Unlike the tests on previous samples, irradiation of “Lyod” was not accompanied by the formation of numerous microscopic spots that lead up to the formation of large scale focal conic structures. Instead, relatively dark blotches start to appear within the irradiated region (*Figure 13b*). After more irradiation, these dark patches then formed disclinations within their borders that were several times larger than the spots seen in previous samples (*Figure 13c* and *13d*). These disclinations are most likely also precursors to the formation of larger focal conic regions, a hypothesis backed up by the image in *Figure 14a*, which shows a distinct focal conic region growing out of one of theses disclinations in the top left corner of the picture (smaller circle) and quite a few smaller focal conic regions within an area full of disclinations (larger circle). These changes are quite drastic when compared to an unirradiated region, depicted in *Figure 14b*. The unirradiated region has none of the blotchy regions, disclinations, or focal conic structures that the irradiated regions have after a just few rounds of testing.

The reason underlying the formation of these localized disclinations, as opposed to the spots that appeared all throughout the samples in previous tests, is probably that the amount of MR dye contained in this thinner sample overall was much smaller than that within the thicker samples. With the thicker samples, the amount of MR likely allowed for continuous adsorbtion of cis MR molecules all throughout the irradiation site, but with the lower amount of MR in ”Lyod”, there was probably not this continuous supply of trans MR molecules that could diffuse to the surface, be isomerized by the pump, and subsequently be adsorbed to the inside surface of the sample. This process likely lead to localized

concentrations of cis MR molecules, which clumped together to form the patchy disclinations shown in *Figure 13b-13d* and *Figure 14a*. This process could have two consequences for the sample "Lyod". First, the creation of these dislinations could affect the macroscopic reflections from the PBG. Ideally, if there are enough of these disclinations and they disrupt reflections from the PBG enough, it should be possible to track these changes with a digital camera. Second, the absorbance of the trans MR isomer in the absorbance spectrum should go down with increasing sample irradiation (since the trans MR molecules would be pulled out of solution and adsorbed to the inside surface of the cell in the cis state).

The results of tracking the macroscopic changes in the sample with a digital camera are pictured in *Figure 16a-16d* and *Figure 17a-17d* on the following page. Overall, the irradiation process doesn't appear to have changed the macroscopic reflections from the sample much, if at all. In these pictures, the irradiated area is shown circled in blue marker on the front of the sample; this is done to make sure the pump laser irradiates the same location during each test. If the disclinations created during testing would have disrupted the PBG enough to cause changes, we would expect to see some of the reflections from the PBG to disappear on the irradiated side (the front side) within the irradiated region (at the

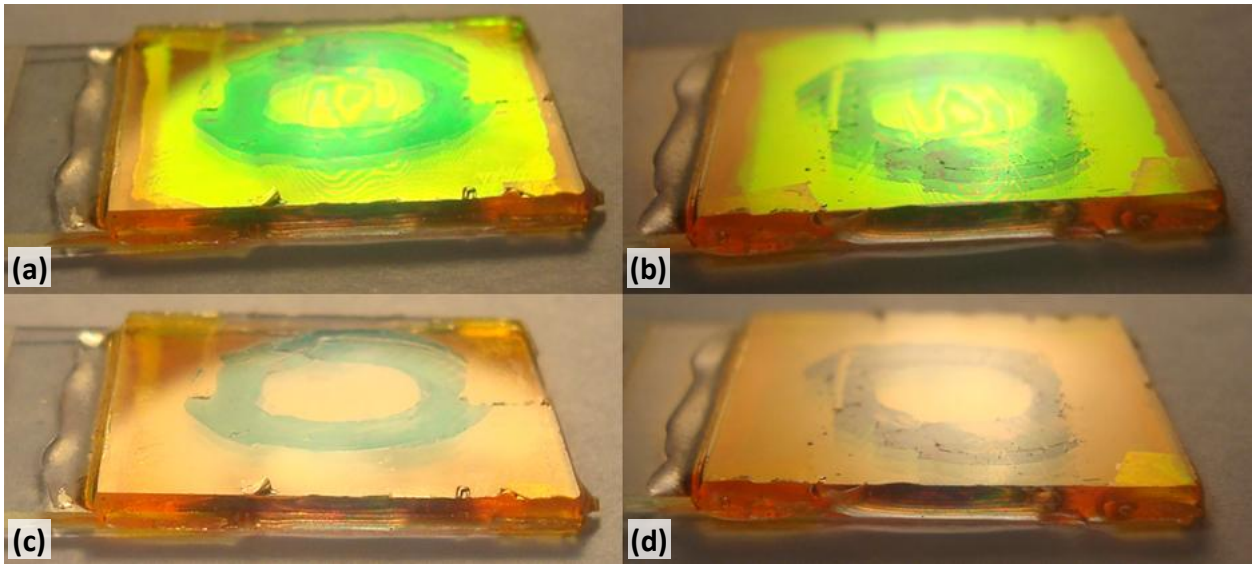

Figure 16: Macroscopic images of sample "Lyod" under different conditions: (a) Front side, right handed filter, initial condition (b) Front side, right handed filter, after Test 09 (c) Front side, left handed filter, initial condition (d) Front side, left handed filter, after Test 09. No discernable changes detected between initial and final condition. (The irradiated area is circled in blue marker to ensure consistency in pump beam placement.)

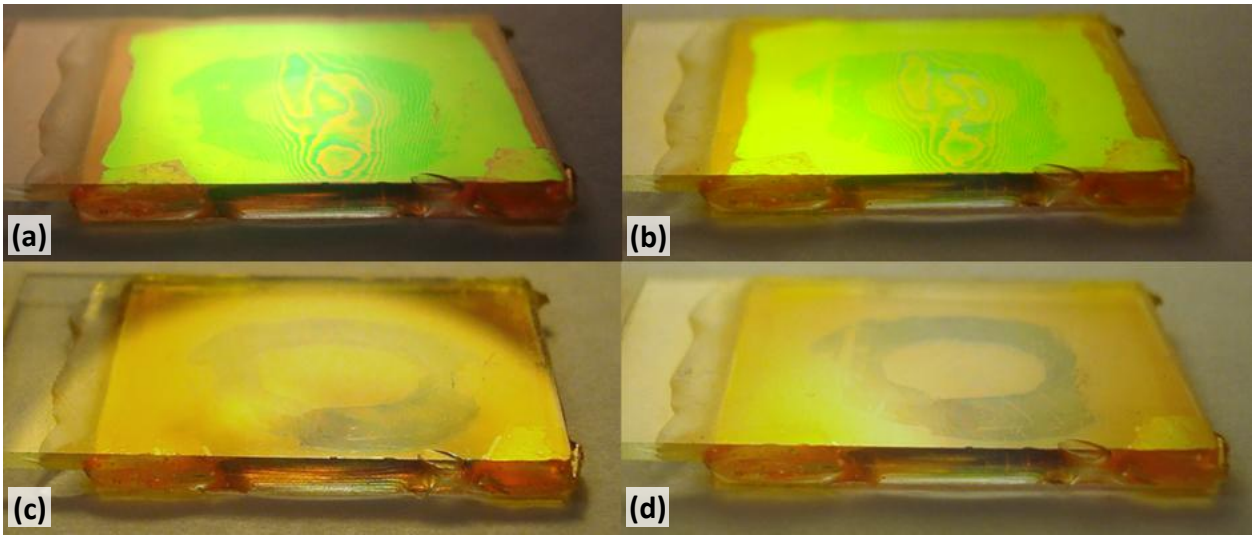

Figure 17: Macroscopic images of sample "Lyod" under different conditions: (a) Back side, right handed filter, initial condition (b) Back side, right handed filter, after Test 09 (c) Back side, left handed filter, initial condition (d) Back side, left handed filter, after Test 11. No discernable changes detected between initial and final condition.

center of the blue circle). The reflections from the PBG are manifested as the green light viewed through the right handed filter. This would mean that some of the reflected green light would go away on the front of the sample, but not on the back, because the back isn't irradiated by the pump and therefore doesn't have cis MR isomers adsorbed there. This is not the case though, so there probably weren't enough disclinations formed during testing to create a macroscopic change in the PBG reflections. Interestingly, for the test on the Instec cell, there was a macroscopically visible loss in PBG reflection on the irradiated side of the sample, but no pictures could be taken of this phenomena because the structure induced by testing was destroyed when the sample was inadvertently heated above its clearing point (the warmth from the microscope light raised the sample's temperature enough to make the CLC go into an isotropic state). The hope for this part of the testing on "Lyod" was to capture this phenomenon, but because of the different nature of the disclinations between the two samples, no such result was seen.

The second physical result that could have resulted from the adsorbtion of cis MR molecules to the inner irradiated surface of the sample was observed though, and in striking detail. It is clear from the

absorbance spectra of both left and right handed light from “Lyod”, that the absorbance of trans MR dye decreases significantly from its initial state through its final state, after test 11. These results are depicted on the following two pages in *Figure 18* for right handed light, and *Figure 19* for left handed light. It is clear from these figures that the absorbance peak for trans MR dye, the peak between 440 nm and 550 nm [9], decreases after nearly every test for both the right and left handed light. This is a result we would expect to see if the trans MR dye molecules were in fact being isomerized to the cis state by the pump beam and then adsorbed to the inside surface of the irradiated region, and it provides strong evidence that this is in fact what is happening.

Importantly, another effect we were looking for arose as a result of testing. The pump irradiation clearly caused shifts in the location and shape of the PBG, as can clearly been seen by the shifting peaks approximately centered around 660 nm in *Figure 18*. The PBG for the thinner samples has a different shape than previous, thicker samples, but this is only due to the relative uniformity in the pitch length brought about by the uniform thickness of the sample. (Less pitch variation equals a smaller band of reflected wavelengths.) Overall, the changes in the PBG for “Lyod” throughout testing were pretty noisy, and this was perplexing at first, since the data should have been better for thinner samples. The reason for this noise was revealed after test 8 though, when the sample was transferred from the relatively cool heat stage, in which irradiation testing had taken place, into the spectrometer setup, which was at room temperature. The PBG was observed shifting quite quickly, and over a significant range, as the sample acclimated to the ambient temperature of the room. To get a better bearing on this phenomenon, tests were run the next day on the same sample that tracked the PBG shift that took place as the temperature of the sample went from 20.1 ^{o}C to 24.9 ^{o}C. These results are shown in *Figure 20* on *Page 42*.

Each line in *Figure 20* represents a new absorbance spectrum taken at 0.014 minute intervals for right handed light from the front of the sample. The older lines, closer to the 20.1 ^{o}C temperature, are

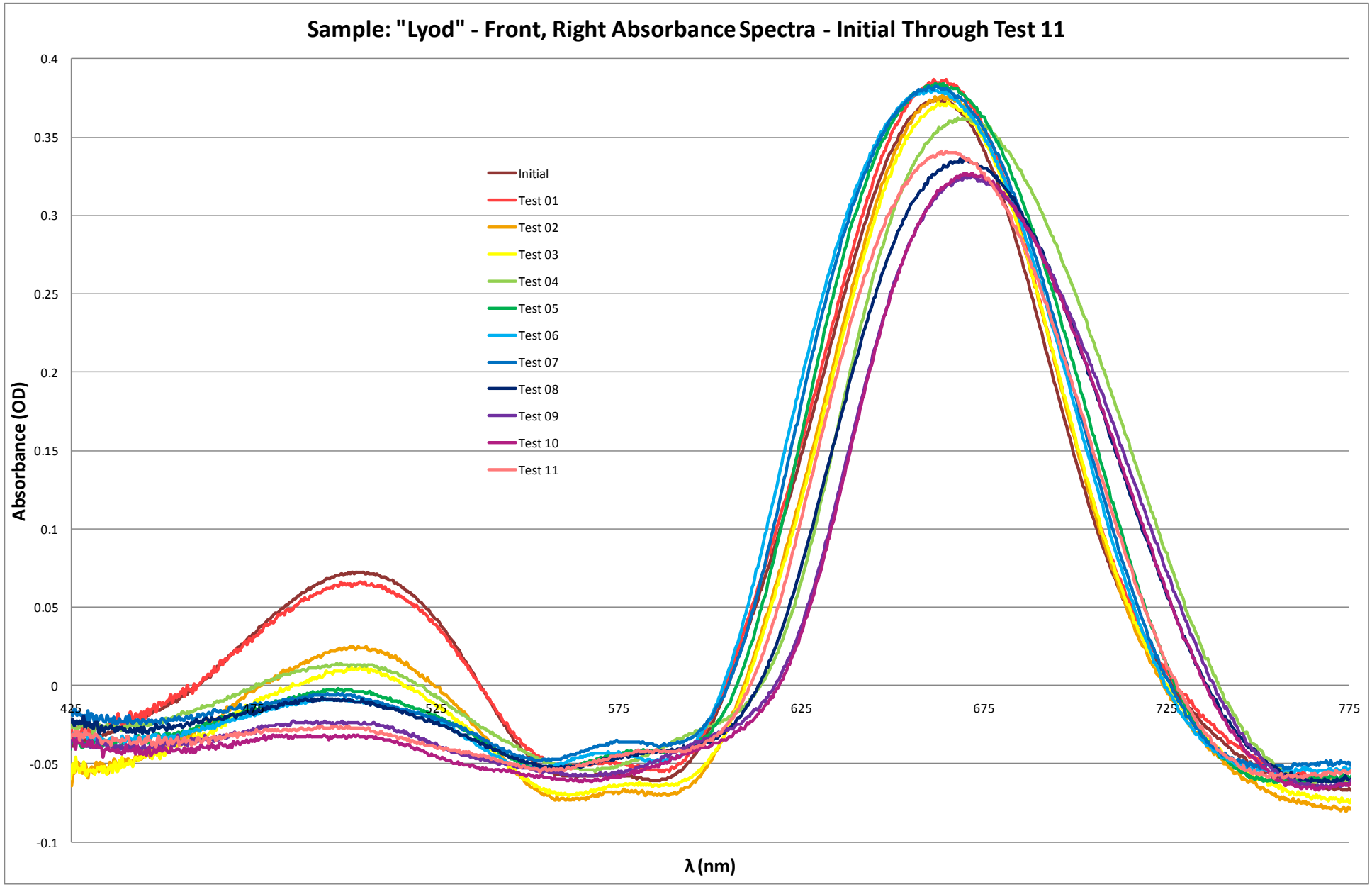

Figure 18: Absorbance spectra profile of the front side of sample "Lyod" for tests 0-11, as measured with right handed light. The PBG is the peak centered around 675 nm, and the absorbtion of the trans isomer of methyl red dye is centered around 500 nm. Changes in the PBG are noisy, but it does appear to shift to the right as testing progresses.

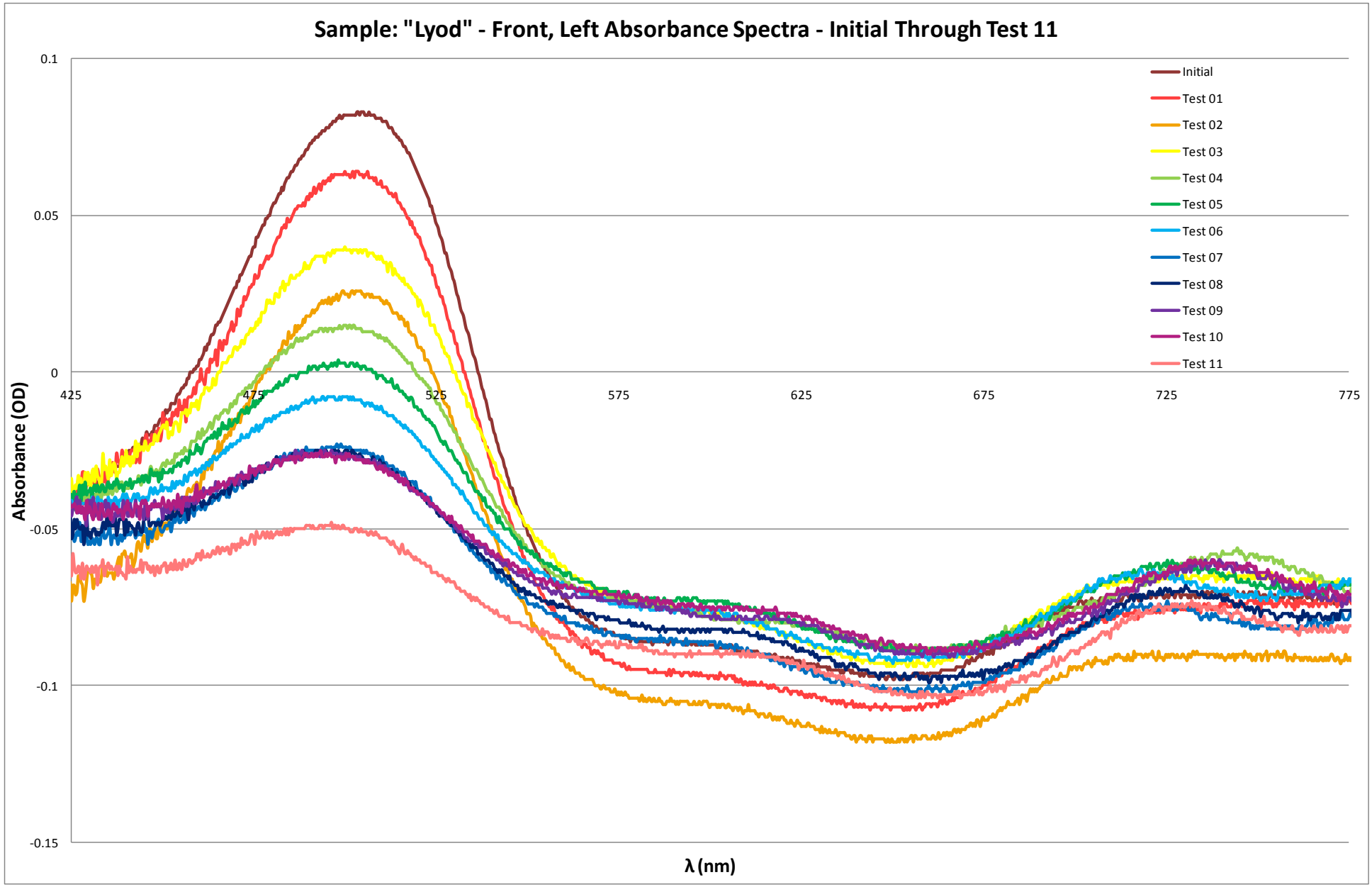

Figure 19: Absorbance spectra profile of the front side of sample "Lyod" for tests 0-11, as measured with left handed light. The PBG is (as expected) not present for left handed light, and the absorbtion of the trans isomer of methyl red dye is centered around 500 nm. The absortion of the trans isomer of methyl red decreases with each test as the pump beam causes more and more methyl red molecules to undergo trans-cis isomerization.

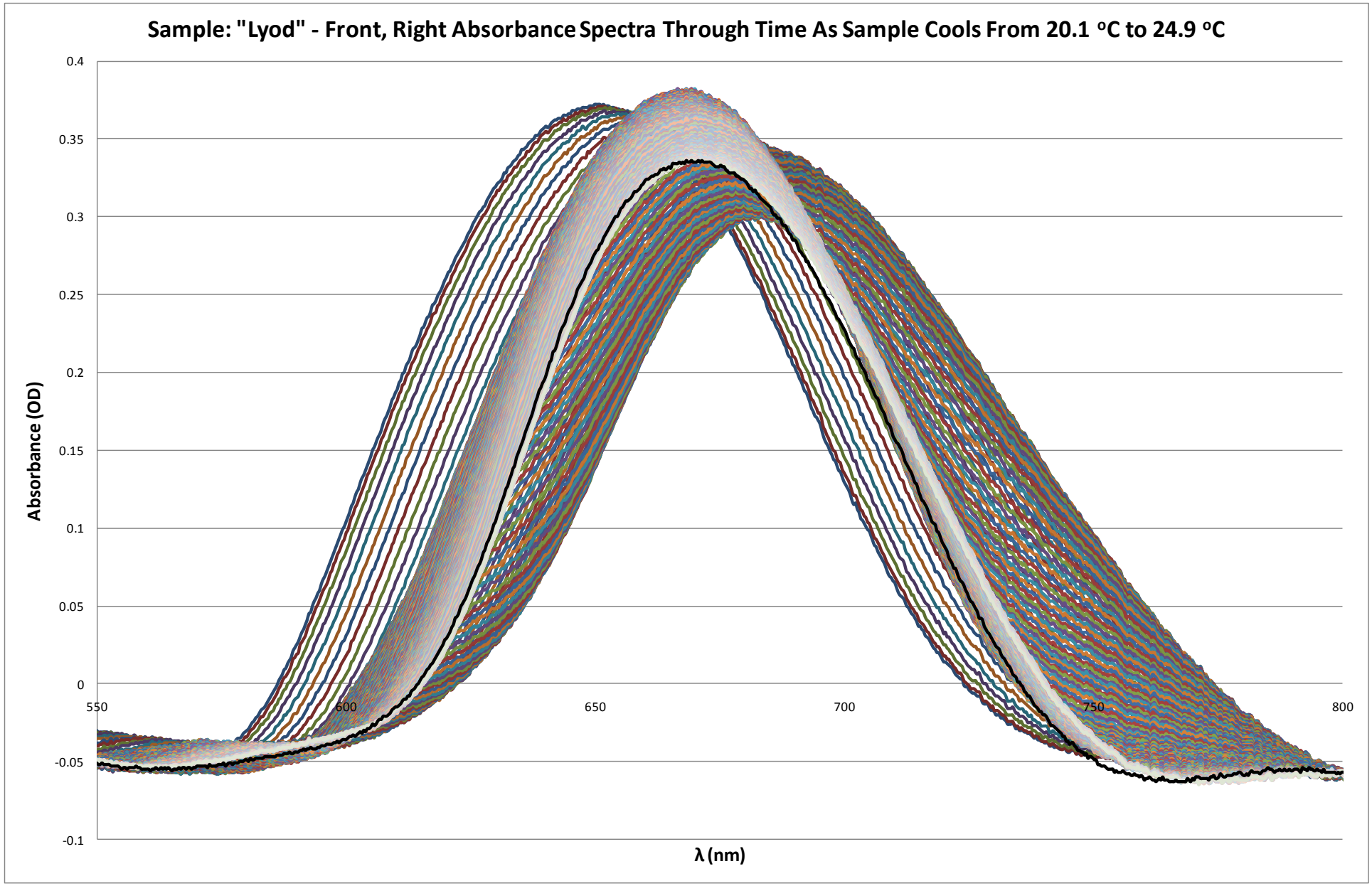

Figure 20: Real time shift of the PBG, as seen from the front of sample "Lyod" with right handed light. As the sample warms to room temperature from 20.1 °C, a spectra was taken every 0.014 minutes and layered over the previous one. The black line (in front) is the stable PBG location, taken after 32.4 minutes. The colored lines span from time 0 to 6.98 minutes. This measurement was conducted one day after the completion of test 08.

layered towards the back while the newer lines, closer to the 24.9 ^{o}C, are towards the front (so that there is effectively a time axis that points out of the figure towards the viewer). This figure shows how the absorbance spectrum of the PBG shifts over 6.98 minutes and ultimately come to rest at the black line, which represents the steady state of the system measured at 32.4 minutes. Essentially what happens it that, as the sample heats up, the PBG shifts rightward from its initial position around 650 nm to 688 nm, after which it starts to shift rightward and then a bit leftward toward its stable value around 668 nm. This process looks pretty complicated, but it is probably due to some pretty simple factors, which will prove to be important for the analysis of the shifts in the PBG caused by irradiation.

What is most likely going on with this temperature induced PBG shift is that thermal expansion is changing the thickness of the sample, which in turn changes the pitch, which subsequently changes the wavelengths of light reflected by the PBG. Analyzing the data collected from the temperature varied PBG, it is possible to see interference fringes moving to the right in the region of the trans MR absorbtion peak as the temperature of the sample rises. The spacing of these fringes can then be used to determine the optical thickness of the sample at 20.1 ^{o}C and 24.9 ^{o}C. (These fringes were hard to see because of layering and the relatively large size of the PBG in *Figure 20*, so the spectra were cropped to make it easier to see changes in the PBG. A figure depicting the initial and final states of the interference fringes can be seen in *Figure 21* though. Even in this figure, however, it can be hard to see the peaks of the fringes, which is why they have been marked with orange circles. It is easier to see the interference fringes in an animated graph showing them moving in time, which is how I was able to pinpoint their position accurately, but such a graphic could not be include here obviously.) Calculating the optical thickness of the sample from the locations of the peaks of these interference fringes (for more on this, see *Appendix A*, *Measuring Sample Thickness*), we get that the initial optical thickness of the sample at 20.1 ^{o}C was equal to 3.15 μm and the final optical thickness of the sample at 24.9 ^{o}C was equal to 3.33 μm. This means that thermal expansion caused the optical thickness of the sample to increase 175 nm.

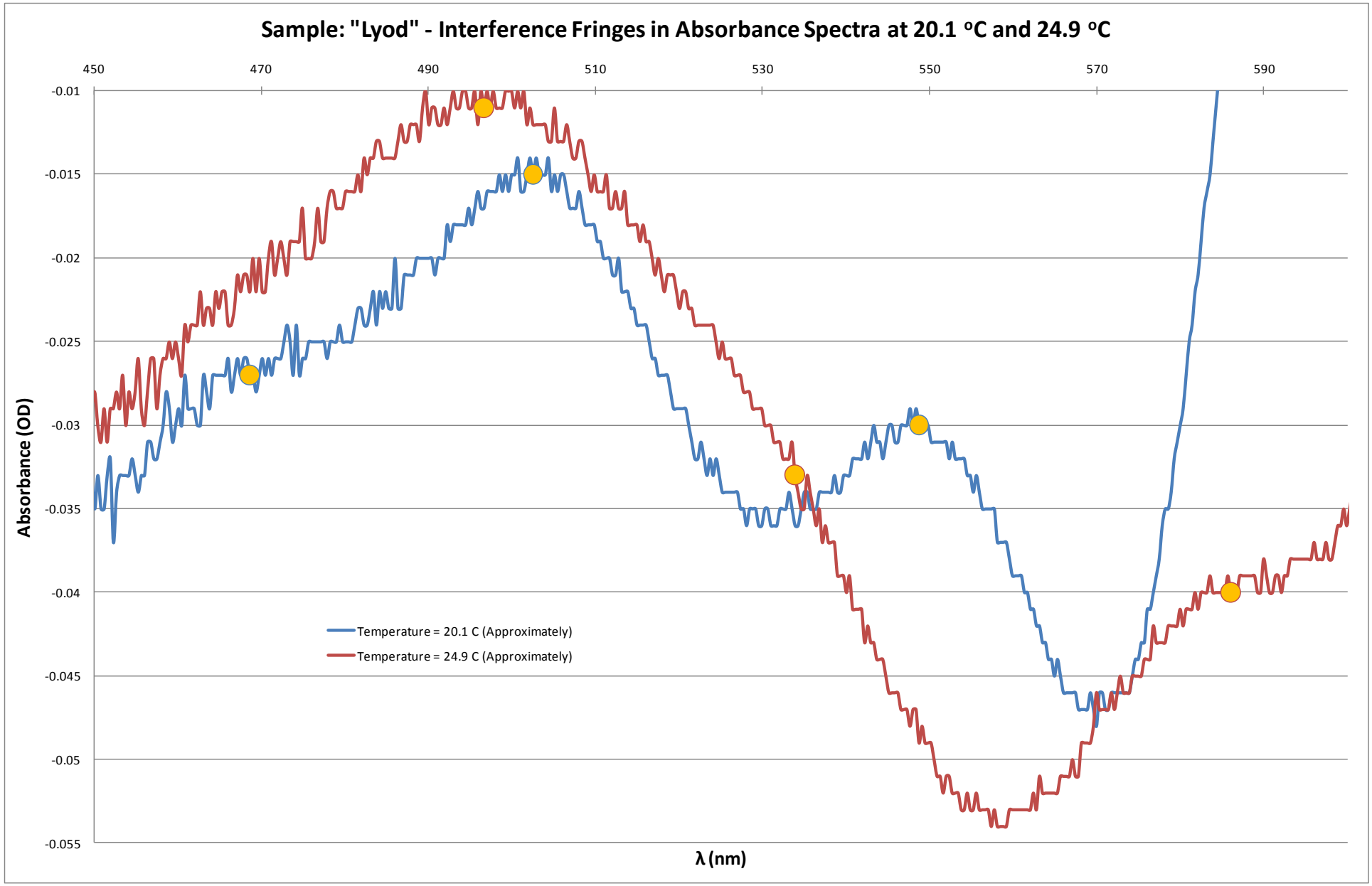

Figure 21: Absorbance spectra for sample "Lyod" at approximately 20.1 °C and 24.9 °C, showing interference fringes moving through the region of the spectrum around the trans MR adsorbtion peak. The peaks of the interference fringes are marked by orange circles. The different spacing of the interference peaks between the initial and final states indicates a change in sample thickness that can be calculated quantitatively.

Since we know that the relationship between optical thickness and actual thickness is

$$d_{actual} = d_{optical}/n \tag{63}$$

where $d_{optical}$ is the optical thickness, d_{actual} is the actual thickness, and n is the average index of refraction (equal to 1.72 for the CLC mixture being used here). Plugging everything in, we get that the thickness of the sample increased by 102 nm while acclimating to room temperature. Furthermore, these results are backed up by the fact that the final actual thickness of the sample, calculated with this method, yields a value of 1.94 μm, which is only off from the unfilled sample thickness of 1.97 μm by 1.52 percent.

This expansion is significant because the thickness of the sample could have increased enough to allow for another half pitch length to fit within the edges of the sample. What we would expect to see if this phenomenon were to occur would be the PBG shifting forward at first. This would occur because the thickness of the sample would be growing and the pitch would correspondingly get longer as a result of this, increasing the wavelengths that the PBG reflects. Remember though, that it is not energetically favorable for the pitch to keep increasing indefinitely because of the bounding conditions described earlier, and when thermal expansion increases the thickness of the sample enough, another half pitch length will be able to fit within the confines of the sample. Passing such a threshold would relieve some of the stress within the CLC structure and allow it to relax to a shorter pitch length (one closer to its equilibrium position) and consequently, this would cause the PBG to reflect shorter wavelengths. After this stage, however, the thickness would start increasing again as thermal expansion continues to drive the sample thickness to larger values, and the process would start all over again.

Note that this whole process is in fact what appears to be occurring in *Figure 20*. The center of the PBG shifts toward longer wavelengths, from 650 nm to 688 nm, but after this point the PBG shifts to smaller wavelengths, around 668 nm, and then starts increasing slowly once more. Remember that the 20 nm shift that occurs when the PBG shifts backwards is a result of each individual pitch length

decreasing in length; any changes in sample thickness affect the pitch only after they get distributed evenly across each pitch length that spans the sample thickness. Since half of the equilibrium pitch length is equal to 190 nm, since the thickness of the sample increased 102 nm (a significant fraction of 190 nm), and since we see, in *Figure 20*, that the PBG behaves as we expect it would under these circumstances, it is reasonable to conclude that another half pitch length is forming in the sample.

All of this information is important because it informs us about what could be affecting the shifts in the PBG measured after testing (*Figure 18*). To get a better idea of how these temperature related shifts in the PBG relate to ones induced by testing, a graph showing an overlay of the two data sets is shown in *Figure 22* on the following page. Obviously the temperature of the sample is a big factor in the location of the PBG, and since the sample was not temperature controlled while absorbance spectra were taken after irradiation tests, it is fair to conclude that variations in room temperature were likely the cause of some of the noise in the PBG shifts (by noisy I mean that the PBG shifted forward a total of seven times and backward a total of four times, with no apparent trend in the series of movements). Even with these variations though, the PBG does appear to have shifted more forward on the whole than backward, and from the overlay in *Figure 22*, it is fair to say that some of these shifts were outside the variability of fluctuations caused by changing room temperature. This is a fair conclusion because the room temperature would have to be close to 20 ^{o}C in order to get the shifts detected for tests 1, 5, 6, and 7, and the room temperature did not vary *that* much.

Even with this knowledge, though, it is not really possible to pin down an exact PBG shift, so it will be prudent to use a range of possible shifts to see how they compare with the theory that has been developed thus far. Taking the shift from the initial spectra to test 10, the PBG moved forward 12.61 nm. Using *Equation 62* and values that were determined earlier, we get that the pump beam would have needed to cause the director on the irradiated surface to rotate 0.61 radians, or 35.08 degrees, to cause the PBG to shift this much. On the other hand, taking the shift from the initial spectra to test 11, the PBG

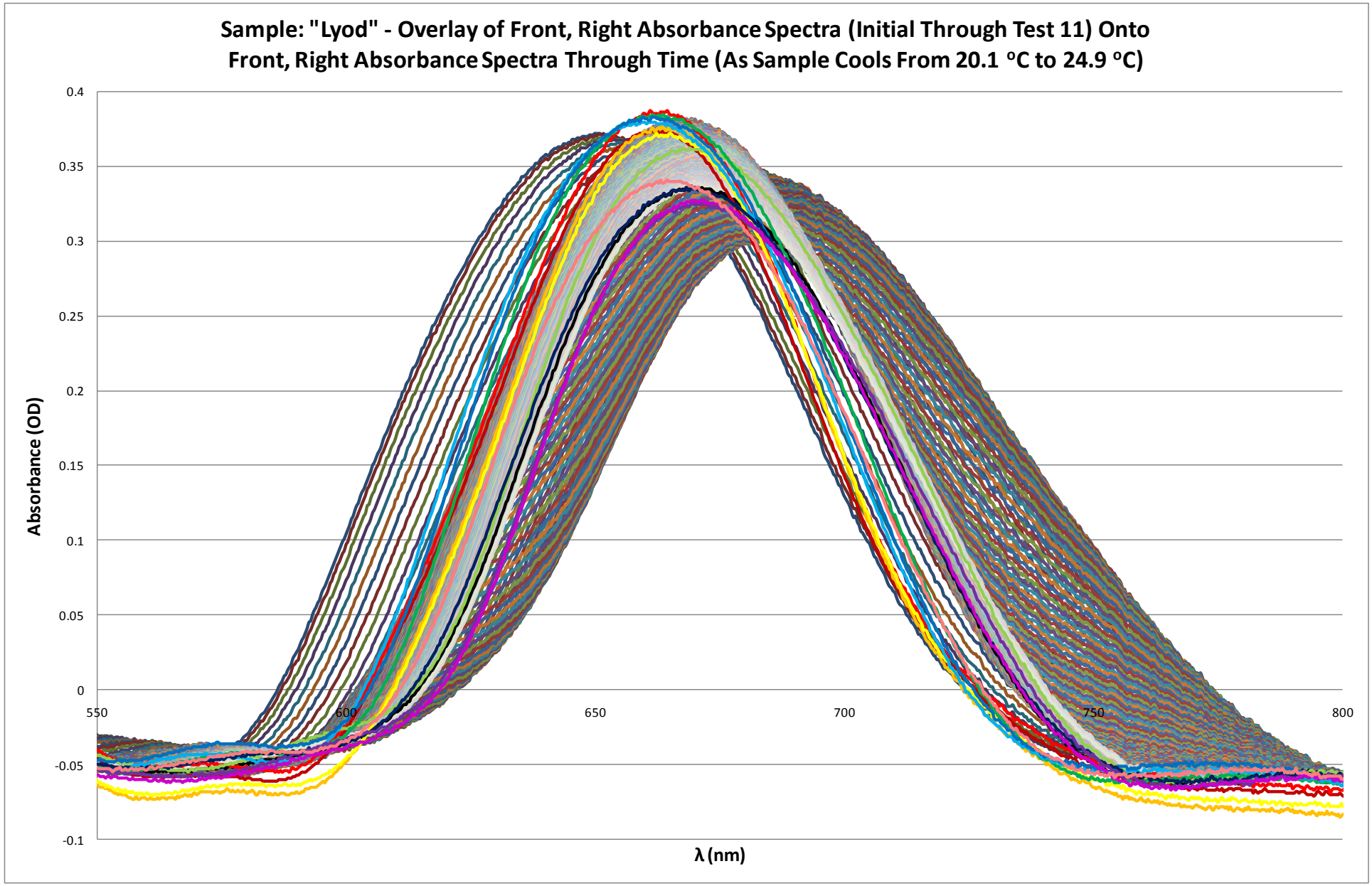

Figure 22: Overlay of irradiation induced shifts measured after each test on "Lyod" over temperature induced shifts measured after test 08 on "Lyod". Although the temperature of the lab was roughly around 25 °C, there was likely enough temperature variation throughout the testing time to give the noisy shifts in the PBG. Still, the PBG does appear to shift toward higher wavelengths throughout the testing period.

moved forward 3.86 nm. Once again, using *Equation 62* and values that were determined earlier, we get that the pump beam would have needed to cause the director on the irradiated surface to rotate 0.19 radians, or 10.74 degrees, to induce such a change in the PBG. (The difference between the initial state and test 10 and test 11 were chosen because they represent the difference between the initial and final states of the PBG.) These two rotations define the range of rotations that needed to have occurred in order to change the PBG in the way observed in *Figure 18*. A rotation between 10.74 degrees and 35.08 degrees seems like a plausible change induced by the pump, since previous experiments have shown that MR dye doped nematic LC samples can rotate up to about 40 degrees, however measuring the actual amount of rotation caused by the pump is tricky for CLC systems.

The measurements in which 40 degree rotations occurred were carried out on non-chiral nematic LC samples doped with MR dye, and irradiation times were much longer than the 900 second irradiation times that were used in these tests. Rotations on the order of tens of degrees may have occurred in the sample "Lyod" though, because the pump intensities used to get large rotations in non-chiral systems fall in the middle of the range of intensities used in these latest tests, and there were quite a few tests conducted on "Lyod", however, measuring director rotations in CLC samples is more difficult than in normal LC samples because the probe radiation comes out of the sample elliptically polarized, making measurements of the changes in linearly polarized light (i.e. the 2nd Stokes Parameter) significantly less meaningful than in non-chiral samples. This means that it was not possible to measure the amount of rotation that the pump caused in the director at the irradiated surface, as was previously hoped, however the data collected on the Stokes parameters can be somewhat useful in analyzing what the pump does to the sample. Some of this data can be found in *Figure 23* on the following page. This figure shows the 2nd and 3rd Stokes parameters collected during the irradiation of "Lyod" from test 8. (Test 8 was included, as opposed to the other tests, because it had a high signal to noise ratio, the changes measured were larger and easier to see than in the other data sets, and because changes in the

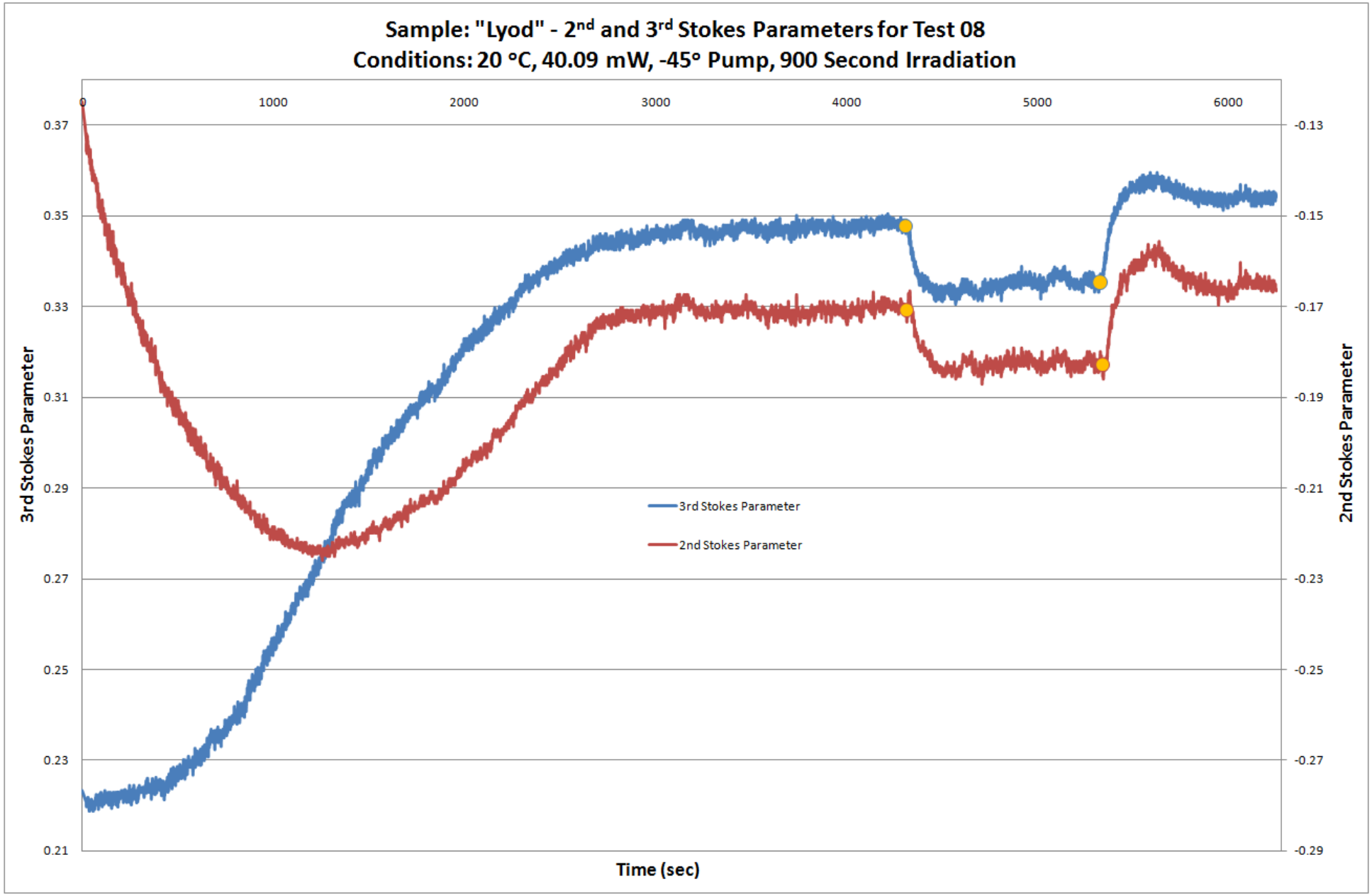

Figure 23: 2SP and 3SP measurements of sample Lyod. Irradiation starts at first orange dot in data and ends at the second. Because of the higher irradiance at test 8, changes in the Stokes parameters arising from the sample's gradual stabilization at 20 °C are do not drown out by changes caused with the pump beam. The profile of the 3SP shows that the pump beam is stressing the CLC structure, as hoped. Not much can be gleaned from the 2SP though.

Stokes parameters of other tests looked very similar to test 8.)

The data in *Figure 23* shows the sample equilibrating to the 20 ^{o}C until the pump beam is turned on at the first orange dot. When this happens, the 3SP decreases, telling us that the probe light passing through the sample has become less circularly polarized. This implies that the helix of the sample has likely been unwound a bit from twisting caused by the pump beam at the irradiated surface, the effect that was desired. After the pump is turned off at the second orange dot, the sample goes back to a value slightly higher than it was before. Also important is the fact that when the pump beam is turned on, and the 3SP gets closer to zero (because the probe beam is becoming less circular), the 2SP goes farther away from zero (becoming more linear in a particular direction). This result is also expected because when the 3SP gets closer to zero, the 2SP should generally get farther from zero. (The 2SP will, however, stay at zero if the polarization of the pump is at a 45 degree angle relative to the coordinates we are measuring it against.) It clear from this that the pump beam is in fact stressing the CLC helix, but using the 2SP to calculate the angle of rotation of the surface director cannot be done.

Conclusion and Discussion

The dynamics of CLC systems are indeed quite complex. Initial testing on such systems gave interesting results that showed the formation of focal conic structures and the partial destruction of the PBG. These were theorized to be the result of the pump beam isomerizing trans MR dye molecules into their cis state, which were subsequently adsorbed to the inner irradiated surface of the sample in such a way that they stuck out into the bulk of the CLC, causing the structures we observed. This result, although interesting, rendered the samples unusable, so methods were changed to allow the sample to be cooled and irradiated at lower intensities, which would then be stepped up gradually to approach the threshold at which focal conic structures appeared. This result still eventually produced the precursors to focal conic structures, but not enough to destroy the sample or the shift in the PBG. The data from "Halitosis" indicated that a 7.04 nm PBG shift had taken place and a surface director rotation of 10.77

radians, or 617 degrees, was necessary to induce such a change, an angle well outside of what our pump beam was capable of achieving. Clearly there was another effect causing shifts in the PBG.

Further calculations indicated that samples with a thickness on the order of 2 μm were required to get a reasonable PBG shift from a rotation that was within the range of our experimental setup. After some work, samples of this thickness were created and tested. Results from this sample indicated that our previous assumptions about the cause of the focal conic structures were accurate, as it was clearly visible that trans MR absorbance decreased markedly with almost every test. Other data about the PBG was not as clear cut though. Shifts in the PBG varied widely, and it was only after nearly all the tests were completed on "Lyod" that it was discovered how much temperature affected the location of the PBG. The shifts caused by temperature were attributed to changes in sample thickness that resulted from thermal expansion as the sample warmed up in the spectrometer setup. Unfortunately, all of the spectra taken after irradiation testing were not conducted in a temperature controlled environment, so this introduced error into the PBG shift measurements. Despite this trouble though, it was reasonably clear that the PBG shifted forward by some amount, although how much was unclear, so a range of the final shifts were taken into account. The real PBG shift for "Lyod" likely lies between 3.86 nm and 12.61 nm, which corresponds to a director rotation between 10.74 degrees and 35.08 degrees. This result lies within the range of rotations that could have plausibly been caused by the pump beam (the limit being around 40 degrees), but whatever factor caused the shifts in the sample "Halitosis" are likely still a factor in the tests on "Lyod" despite its significantly smaller thickness and high uniformity. Unfortunately though, the degree to which this mystery factor comes into play in *these* measurements cannot be determine as of yet because the Stokes parameter measurements do not provide sufficient information to determine the amount of rotation caused in the director, they only tell us that the CLC helix is being stressed by the torque exerted by the optical field of the pump beam.

There should be a way, however, to determine how much of a role this mystery factor plays in

shifting the PBG, thanks to Dr. David Statman. After some deliberation, we determine that this factor likely results from the formation of cis MR dye molecules close to the irradiated surface during its exposure to the pump beam. This could cause a shift in the PBG because cis MR dye molecules are likely somewhat chiral themselves, as a chiral cis MR dye molecule would most likely reduce the steric interaction of its benzene rings and would therefore be a more energetically favorable configuration. These new chiral molecules could likely act as another chiral doping agent within the sample, effectively increasing or decreasing the chirality of the CLC sample, and therefore changing its pitch length and PBG. To test this, his suggestion would have future tests run on a CLC sample with the pump beam parallel to the director, so that any rotational effects on the PBG can be eliminated, leaving only the interactions of the isomerized MR dye molecules to change the structure of the sample.

Future Work

The results from this past year, although not conclusive, are very intriguing and they can be used to guide further research on this topic, and there is indeed a great deal of future work available for this project. For starters, the Stokes parameter tests showed significant intensity dependence; something that should have been cut out by taking the ratio of the photo detector's signal voltage to it RMS voltage. Despite numerous hours of work, this problem could not be alleviated. Correcting this problem would allow for better information on the actual starting and end points of the 2SD and 3SP for each set of tests on a sample, and allow for more accurate overall measurement of the Stokes parameters.

More work also needs to be conducted to explore the formation of focal conic textures in these CLC cells. Preliminary tests on thicker cells at longer irradiation times undoubtedly produced the focal conic structure within samples; however I was unable to reproduce these effects in my thinner samples, but this may have been the result of a lower overall amount of MR dye molecules in the thinner sample, the lower irradiation times, or maybe something altogether different. Nevertheless, these results need to be explored because they shed light on what may be going on within the sample during the

irradiation process.

Another area in need of improvement and future work is the spectrometer measurements. Variations in sample orientation were eliminated as a cause for significant error in the spectrometer measurements through the construction of a better sample holder, however (as is evidenced in *Figure 20*) the spectrometer readings for each test need to be conducted within the temperature controlled sample holder, as fluctuation in room temperature have a significant effect on the measured position of the PBG. Lab equipment will need to be reconfigured for such a task. Furthermore, reconfiguring the setup so that spectra of a sample can be taken in the same location that it is irradiated by the bump beam will allow for measurements immediately after the pump beam is turned off and will eliminate the need to transfer the sample or the heat stage from setup to setup. This would be a significant advancement because it would allow for information to be taken without exposing the sample to varying temperatures (which cause significant error) and for information to be gathered about how the PBG behaves immediately after exposure to the pump (this could help discredit or confirm the theory the cis isomer of MR acts as a chiral doping agent).

A few more possible experiments that may corroborate the conclusions of this project include testing whether or not greater temperature changes will lead to more of the fluctuations (seen in *Figure 20*) and more of the changes in the number of pitch lengths contained within the sample. Also, tests should be run which measure changes in the 2SP and 3SP as the temperature is varied. This could likely lead to more evidence supporting our conclusions about how temperature affects the sample. Finally, one of the most important experiments that needs to be conducted is the vertical pump beam test described earlier. This should help clarify what is going on, aside from director rotation, within the CLC sample.

References

[1] Khoo, Iam Choon. "Nonlinear Optics of Liquid Crystalline Materials." Physics Reports 471.5-6 (2009): 221-67.

[2] Jánossy, I., and L. Szabados. "Optical Reorientation of Nematic Liquid Crystals in the Presence of Photoisomerization." Physical Review E 58.4 (1998): 4598-604.

[3] Serak, S., A. Kovalev, and A. Agashkov. "Laser-induced Surface and Bulk Reorientation of the Director in Azo-dye-doped Liquid Crystal Cells." *Optic Communications* 187 (2001): 235-47.

[4] Simoni, F., and O. Francescangeli. "Effects of Light on Molecular Orientation of Liquid Crystals." *J. Phys.: Condens. Matter* 11 (1999): R439-487.

[5] Schadt, Martin, Klaus Schmitt, Vladimir Kozinkov, and Vladimir Chigrinov. "Surface-Induced Parallel Alignment of Liquid Crystals by Linearly Polymerized Photopolymers." *Japanese Journal of Applied Physics* 31.Part 1, No. 7 (1992): 2155-164.

[6] Collings, Peter J., and Michael Hird. *Introduction to Liquid Crystals Chemistry and Physics*. London: Taylor & Francis, 1997.

[7] Faetti, Sandro, and Prisca Marianelli. "Azimuthal Director Gliding at a Strongly Anchoring Interface of Polyimide." Liquid Crystals 33.3 (2006): 327-34.

[8] Chandrasekhar, S. *Liquid Crystals*. Cambridge: Cambridge Univ., 2004.

[9] Cheng, Ko-Ting, Cheng-Kai Liu, Chi-Lun Ting, and Andy Y. Fuh. "Electrically Switchable and Optically Rewritable Reflective Fresnel Zone Plate in Dye-doped Cholesteric Liquid Crystals." *Optics Express* 15.21 (2007): 14078.

Griffiths, David J. *Introduction to Electrodynamics*. Upper Saddle River, NJ: Prentice Hall, 1999.

Hecht, Eugene. Optics. Boston: Addison-Wesley, 2002.

White, T., Freer, A., Tabiryan, N., Bunning, T. (2010). Photoinduced broadening of cholesteric liquid crystal reflectors. *Journal of Applied Physics*, 107, 073110-1 - 073110-6. doi:10.1063/1.3369437

Appendix A - Sample Preparation

Cleaning:

(1) Pre-cleaned glass slides were cut into 3.7 cm and 2.6 cm long pieces (a pair of these make one cell).
(2) Cut glass was cleaned with Alconox.
(3) Two sets of these cut, cleaned slides were placed into a 50 mL beaker with magnetic spacers separating them to keep them from touching.
(4) Beaker full of slides was rinsed with DI water 3 times.
(5) Beaker full of slide was filled with DI water and placed into a Branson 2510 sonicator for 15 minutes.
(6) Steps (4) and (5) were repeated except beaker was filled with 1 M NaOH this time.
(7) Steps (4) and (5) were repeated except beaker was filled with isopropyl alcohol this time.
(8) Steps (4) and (5) were repeated except beaker was filled with DI water this time.
(9) Cleaned cells were dried with compressed nitrogen gas.

Making PI Solution:

(1) 2 mL of toluene and 8 mL of 1-methyl-2-pyrrolidone were mixed.
(2) 9 mL of the mixture from (1) was combined with 3 mL of polyimide (PI) (PI2555).

Spin Coating:

(1) A cleaned glass slide was placed into homemade spin coating machine, built out of a rotating stage attached to a motor, powered by a variac.
(2) Slide was spun for 1 minute at 56 V to remove dust and other particles.
(3) PI was pipette onto slide in a repeating S patern until the majority of the slide was coated in a thin film of the polymer.
(4) Spin coater was run for 4 minutes at 56 V to evenly coat slide and spin off excess polymer.
(5) Slide was then removed and excess polymer was removed from its underside with isopropyl alcohol.
(6) Process was repeated for each slide.

Curing (Baking) PI

(1) All PI slides were baked together at once in a Black and Decker toaster oven at 90 ^{o}C for 15 minutes.
(2) Temperature was then turned up to 150 ^{o}C for 60 minutes.
(3) Slides were taken out of oven to let them cool overnight.

Rubbing Slides

(1) Slides were rubbed 5 times along the long axis of the glass slide with a homemade rubbing device covered in velvet. (For the shorter glass slides, rubbing was toward the cut end so that the rubbing direction could be easily remembered.)

Cell Assembly

(1) Four 5 μm thick Mylar spacers were cut in the shape of small squares and placed onto the corners of the PI coated side of 2.6 cm slide.
(2) The 3.7 cm glass slide was placed on top of the 2.6 cm slide so that the polymer surfaces faced each other and their rubbing directions were parallel.
(3) ***Very Important!*** 4 green clip clamps were placed about half way between each corner and the center of the cell. Their position was modified to make the central interference fringes of the cell as

uniform as possible.

(4) Epoxy was then mixed and applied to the 2 outside edges of the cell parallel to its long axis. (The 2 µm thick cells were made with quick drying, 5 minute epoxy. The quick dry time kept the epoxy from entering the cells too much.)

(5) The cells were allowed to set overnight. Clamps were left on overnight, as this actually helped the samples attain a thickness smaller than that of the spacers.

Measuring Sample Thickness

(1) Transmission tests were run using SpectraSuite and the setup pictured in *Figure 24* to determine the thickness of each sample.

(2) The transmission spectrum of the empty cell was recorded and analyzed to determine the thickness of the cell using the following relationship

$$d = \frac{1}{2}\frac{(\lambda_1\lambda_2)}{(\lambda_2 - \lambda_1)} \div 1000 \tag{64}$$

where λ_1 and λ_2 are adjacent maxima near 100% transmittance, and d is the thickness of the cell in micrometers.

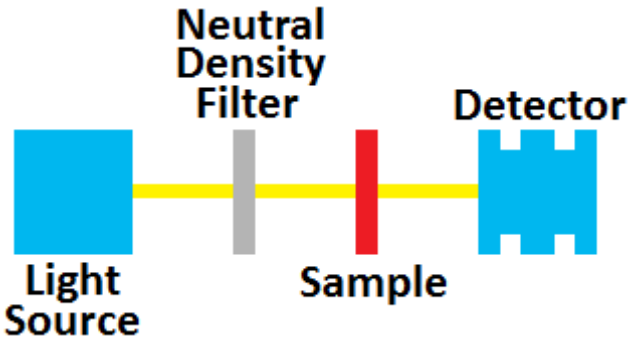

Figure 24: Setup for measuring the thickness of a sample cell while it is empty. The neutral density filter's purpose is to ensure that the detector doesn't saturate.

Doping the LC

(1) Doping the liquid crystals with chiral doping agents or dye was done by weight on a very accurate electronic scale. Very small weights of liquid crystals, doping agents, and (especially) dyes are needed to make a sufficient amount of dye doped CLC sample.

(2) Heating, shaking, and sonicating may be required to fully mix and dissolve all the components of a freshly made sample of dye doped CLC sample.

Filling Cells

(1) A miniscule amount of CLC sample was pipette onto the 3.7 cm slide where it meets the 2.7 cm slide and forms a lip (capillary action pulls the CLC into the cell).

(2) Once the cell was completely filled, the remaining open sides of the cell were sealed with 5 minute epoxy.